Granule Formation, Structure and Content Uniformity from Single Drop Impact on

Heterogeneous Powder Beds

by

Tianxiang Gao

A Dissertation Presented in Partial Fulfilment
of the Requirements for the Degree
Doctor of Philosophy

Approved April 2020 by the
Graduate Supervisory Committee:

Heather Emady, Chair
Nikhilesh Chawla
Yang Jiao
Shankali Pradhan
Sarang Oka

ARIZONA STATE UNIVERSITY

May 2020

ABSTRACT

Single drop impact of liquid on a static powder bed was studied to investigate the granule formation mechanism, droplet penetration time, the characterization of granules (morphology, surface structure and internal structure), as well as the formation regime map. Water was used as the liquid and two pharmaceutical powders, microcrystalline cellulose (MCC) and acetaminophen (APAP), were mixed to make heterogeneous powder beds. The complete drop impact and penetration was recorded by a high-speed camera. Two granule formation mechanisms identified previously occurred: Spreading and Tunneling. Spreading occurred for mixtures of large particle sizes, while Tunneling started to occur when the particle sizes of the mixtures decreased. With an increase of APAP concentration, the overall drop penetration time increased, which was in good agreement with previous literature. The granule morphology, surface structure, and internal structure were characterized by a prism method with image analysis, scanning electron microscope, and X-ray microtomography, respectively. The Spreading mechanism produced flat disks with porous internal structures, while the Tunneling mechanism produced round granules with dense internal structures. Granules that were formed via a hybrid of the mechanisms, Spreading/Tunneling, were hybrid granules, with some dense areas and some porous areas. The results of the granule content uniformity from UV-vis spectrometry revealed that with the increase of APAP proportion, the overall uniformity was compromised for mixtures with fine ingredients, while the content was much more uniform for coarse mixtures. It is

i

believed that the mean particle size of the powder bed is the predominant factor in influencing the formation mechanism, drop penetration time, and granule properties, while the content uniformity is affected by both the particle sizes and the mixture hydrophobicity.

ACKNOWLEDGEMENTS

TABLE OF CONTENTS

LIST OF FIGURES

LIST OF TABLES

CHAPTER 1. INTRODUCTION

Wet granulation is the process of adding liquid binder to particles to form enlarged granules, achieving improved particle properties. It is applied widely in pharmaceutical, foods, agricultural, catalyst and detergent chemical industries. The size-enlargement process equipment involved in granulation include tumblers, mixers and fluidized beds.

Among the wet granulation processes, single drop granulation is the ideal operating regime, where one drop forms one granule. It is a drop controlled nucleation regime that is separated from other rate processes [1,2], so that the best control of granule properties can be achieved.

Wet granulation is considered as an example of design. To achieve desired attributes of the granule product, both formulation properties (powder and liquid) and granulation process design (type of granulation and operating parameters) need to be chosen well [3]. A good particle design requires: knowing clearly required granule properties, good characterization of the powder and granules, and understanding how formulation properties and processing parameters affect the granules [4].

Microcrystalline cellulose (MCC) and acetaminophen (APAP) are used as one case study powder system. These are common pharmaceutical materials, as MCC is an excipient while APAP is an active ingredient (API). We want to investigate how the particle size, contact angle with water and relative proportions of each component will affect the

granulation process and granule products, which is an important area of research in industrial pharmaceutical manufacturing.

The thesis objectives of this research include:

1. Investigate the effects of formulation properties like particle size distribution and particle contact angle with liquid binder on the wet granulation process for the complex MCC-APAP powder system.

   ➢ Examine the drop penetration time and granule formation mechanisms.

   ➢ Characterize the granule morphology, internal structure and content uniformity.

2. Establish a granule formation mechanism regime map for the MCC-APAP powder system and use it to predict and design the granulation process and granule attributes for this and other complex powder mixtures.

CHAPTER 2. LITERATURE REVIEW

2.1. Background

Wet granulation is a process by which agglomerates are formed using liquid to bind particles together. The wet granulation process includes three basic stages: wetting and nucleation, consolidation and growth, and granule attrition and breakage, which occur simultaneously [3]. Among all of the stages, the wetting and nucleation stage is the focus of this study, where the interaction between the liquid binder and the powder occurs. The wetting and nucleation behavior is dependent on several parameters of the powder substrate: the particle size distribution, packing of the powder, and wettability of the powder surface. Whether the binder can wet the powder well is critical to indicate the performance of the wet granulation. This wetting ability can be characterized by the drop penetration time and granule formation mechanism, influencing the granule properties (e.g., morphology, structure, and content uniformity).

2.2. Drop penetration time

The drop penetration time is defined as the time that the drop penetrates thoroughly into the powder bed. The drop penetration time directly shows if the binder can wet the powder bed easily or not. Researchers have been studying the penetration time for decades.

Drop penetration time of droplets into porous materials was first modelled by Middleman [5]. The drop penetration time (also known as wicking time) model was written as:

$$\frac{\sigma t_w}{\mu V_0^{1/3}} = \left(\frac{1.37 V_o^{\frac{1}{3}}}{\varepsilon^2 R_{pore} cos\theta_d}\right)$$

(1)

where R_{pore} is the pore size of powder bed, σ is the surface tension of the liquid, t_w is the wicking time, V_0 is the initial volume of the drop, μ is the drop viscosity, ε is the powder bed porosity and θ_d is the contact angle. The drop penetration time thus depends on the initial drop size, liquid viscosity, and properties of the porous medium.

Two cases of drop penetration behavior were defined by Marmur et al. [6], and are illustrated in Fig. 2.1. The first is the constant drawing area (CDA) case, where the drop diameter remains constant while the apparent contact angle decreases as the droplet penetrates into the powder bed (see Fig. 2.1a). This is the most common case, and the drop penetration time for the CDA condition is defined by [1] as:

$$\tau_{CDA} = 1.35 \frac{V_o^{2/3}}{\varepsilon^2 R_{pore}} \frac{\mu}{\gamma_{LV} cos\theta_d}$$

(2)

where τ_{CDA} is the theoretical penetration time for CDA, which depends on the initial drop volume, V_0, the bed porosity, ε, the pore size, R_{pore}, the liquid surface tension, γ_{lv}, and the liquid viscosity, μ. The other case was defined as the decreasing drawing area (DDA) case, where the apparent contact angle remains constant during the penetration, while the liquid contact area decreases to the center (see Fig. 2.1b). The τ_{DDA} was measured to be 9 times

4

slower than τ_{CDA} [7] due to the fact that in the DDA case, as the drawing area decreases, the pores under the droplet also decrease, which slows down the penetration.
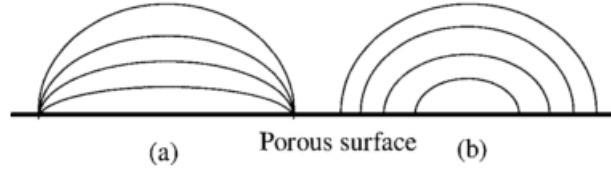
Figure 0.1. Limiting cases of drop penetration on a porous surface: (a) Constant drawing area (CDA) case, with a constant drop radius and decreasing contact angle with time. (b) Decreasing drawing area (DDA) case, where the contact angle remains constant and the drop radius decreases with time [1].

In powder systems, the pore size, R_{pore}, was defined by the Kozeny approach and refined by Hapgood et al.[1] as:

$$R_{pore}=\frac{\emptyset d_{32}}{3}\frac{\varepsilon}{1-\varepsilon} \tag{3}$$

where $\emptyset$ is the particle shape factor and d_{32} is the particle surface mean diameter. However, this equation works well only for well-packed pores in homogeneous beds [1]. In some granulators that contain loosely packed powder and heterogeneous pore sizes, there may be large macrovoids that could suddenly widen the general pore size. This effect would largely inhibit the flow of the liquid inside the powder bed. To include the macrovoids, Hapgood et al. [1] then refined the pore size Eqn. (3) by considering tap porosity and macrovoids porosity. The new effective porosity, ε_{eff}, is defined as:

$$\varepsilon_{eff}=\varepsilon_{tap}(1-\varepsilon_{macrovoids})=\varepsilon_{tap}(1-\varepsilon+\varepsilon_{tap}) \tag{4}$$

where ε is the bed voidage, ε_{tap} is the tap voidage and $\varepsilon_{macroviods}$ is the macrovoids voidage

Substituting the new effective porosity into Eqn. (3), we get a new effective pore size, R_{eff} [1]:

$$R_{eff} = \frac{\emptyset d_{32}}{3} \frac{\varepsilon_{eff}}{1 - \varepsilon_{eff}} \tag{5}$$

Thus, a new drop penetration model was established, including the effective porosity and effective pore size [1]:

$$\tau_{CDA} = 1.35 \frac{V_o^{2/3}}{\varepsilon_{eff}^2 R_{eff}} \frac{\mu}{\gamma_{LV} cos\theta_d} \tag{6}$$

This model is valid for hydrophilic powder systems. However, in the food and drug industries, many particles tend to be hydrophobic. Hence, granulation with different wettability limits needs to be investigated. Based on the previous model in Eqn. (6), the same research group [8] modified the model for systems with hydrophobic ingredients. The ingredients in their study were mixtures of two grades of salicylic acid and two grades of lactose monohydrate, as the hydrophobic and hydrophilic components, respectively. Since the hydrophobic parts would affect the penetration area and flow of the liquid through capillaries, the hydrophobic regions should be considered where the flow would slow down and the penetration would be inhibited. In the new model, to take into account the hydrophobic regions, a ratio of hydrophobic particle surface area, fSA_{phobic}, to the total surface area of the powder mixture, SA_{blend}, was considered [8]:

$$\varepsilon^*_{eff} = \varepsilon_{tap}\left(1 - \varepsilon_{macrovoids} - \varepsilon_{hydrophobicity}\right) = \varepsilon_{tap}\left(1 - \varepsilon + \varepsilon_{tap} - \varepsilon\frac{fSA_{phobic}}{SA_{Blend}}\right) \tag{7}$$

6

Incorporating the modified effective porosity ε^*_{eff} into Eqn. (6) gives the new drop penetration model [8]:

$$\tau_{CDA} = 1.35 \frac{V_o^{2/3}}{((1-\beth)\varepsilon^*_{eff})^2 R_{eff}} \frac{\mu}{\gamma_{LV} cos\theta_d} \tag{8}$$

where $\beth$ is the parameter that represents the proportion of powder surface area that consists of hydrophobic components. Based on their results, finer powders have longer drop penetration times on average compared to coarser powder mixtures. There is also a critical concentration of the salicylic acid where a transition from hydrophilic penetration behavior to hydrophobic penetration behavior occurred. The granules made from mainly hydrophilic components have a larger size and appear to be stronger than those made from more hydrophobic powders. The revised model was also able to improve and predict the drop penetration time, especially for much longer penetration times.

Several researchers also used and verified Hapgood's drop penetration model from Eqn. (6), while Eqn. (8) has not been validated in the published literature. Kayrak-Talay et al. [9] verified the drop penetration model by investigating granulation with polyvinylpyrrolidone (PVP) solution on lactose/acetaminophen and confirmed the relationship between penetration time and particle size and contact angle. From the results, the drop penetration time increased with the decrease of particle size. The addition of 5% by weight of acetaminophen and crospovidone into the formulation that comprised 95% lactose resulted in a large increase in drop penetration time. This is due to the increase of

7

contact angle between the added components with the PVP solution. A drop diameter of 100 μm was also used to replace the single drop size of 2.91 mm based on Eqn. (6) to simulate the results in spray nozzle granulation, where the typical drop diameter would be 100 μm. Based on the penetration time results, both lactose particles with large size differences and formulation composition changes have significant effects on drop penetration time. Oostveen et al. [10] conducted a validation of the Hapgood model in Eqn. (6) on food starch powders. The experimentally measured drop penetration time was compared with theory. It was found that the internal porosity and the moisture level of the powder have an effect on drop penetration time. To improve the fitting of the results to the theory, the effective porosity was replaced by an experimentally determined pore size. During the penetration experiment, the penetration area exceeded the drawing area when the droplet impacted the powder surface initially (see Fig. 2.2).
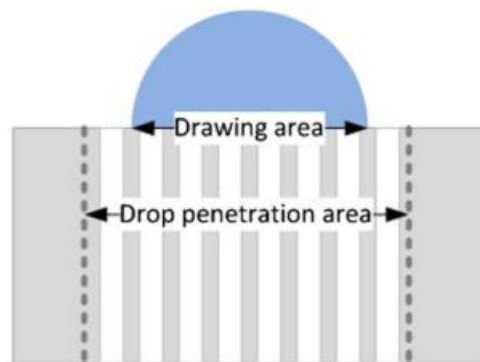
Figure 0.2 Schematic of a water droplet on a corn starch powder bed [10].

It was visually observed via the drop size estimation of the video frames that the actual penetration area was about 1.5 times larger than the drawing area. This could lead to a

larger effective porosity and finally a shorter penetration time. Besides this area factor, the true internal pore size obtained experimentally by micro-CT is larger than that obtained from Eqn. (5). From their results, the incorporation of the experimentally measured pore size gave a better fit to the theory model from Hapgood.

Hapgood's model in Eqn. (6) was used to characterize the penetration time of other power-liquid systems as well [11–14]. Marston et al. [13] researched drop spreading and penetration on dry and pre-wetted glass beads. They studied both the dynamics of spreading and penetration time. Moisture level and drop height, which gives different impact speeds, were investigated. for dry powder, the apparent contact diameter was constant during the penetration, while for pre-wetted powders, the diameter decreased with time and finally diminished. for dry powder, the penetration time was independent of impact speed. The fastest penetration was achieved at a moisture content of 5% in experiments. A calculated penetration time, t_{CDA}, had a minimum at a moisture content of 5.4%, which was in good agreement with their experimental results. This leads to the conclusion that the penetration times for pre-wetted powders are shorter than for dry powders. on the contrary, Charles-Williams et al. [14] found that the drop penetration times into pre-wetted powder are much longer than into dry powder. They performed single drop granulation on lactose monohydrate powders of three size grades (11 μm, 27 μm and 115 μm) by three binders with different liquid properties, particularly viscosity and surface tension. They found a competitive spreading against infiltration process, where the

infiltration rate is highly dependent on the liquid viscosity compared with spreading, where decreasing the liquid viscosity causes a faster infiltration rate than the spreading rate during the drop penetration.

The drop penetration time models and the materials used from the literature are summarized in Table 2.1.

Drop penetration model	Material	Primary particle size (μm)	Liquid binder	Reference
τ_{CDA} $= 1.35 \dfrac{V_o^{2/3}}{\varepsilon^2 R_{pore}} \dfrac{\mu}{\gamma_{LV} cos\theta_d}$	Sands, soil	N/A	N/A	[1]
	Lactose monohydrate	11/27/115	Water, PVP solution, PEG solution	[14]
τ_{CDA} $= 1.35 \dfrac{V_o^{2/3}}{\varepsilon_{eff}^2 R_{eff}} \dfrac{\mu}{\gamma_{LV} cos\theta_d}$	Glass ballotini	29.61/113.4	Water, HPC, PEG, lactose solution	[1]
	Lactose	64.43/17.86		
	ZnO, TiO$_2$	1.25/0.73		
	Pure lactose	45.9/17.9/12.9/12.2/9.1	PVP solution	[9]
	Lactose-based formulation	N/A		
	Food starch	13.22/34.57/18.52	Distilled water	[10]
	Glass beads	72.36		
	Porous silica	90.0		
	Glass beads	42/98/165	Ethanol-water solution	[11]
	Salicylic acid	13/429		[8]

$\tau_{CDA} = 1.35 \dfrac{V_o^{2/3}}{((1-\beth)\varepsilon^*_{eff})^2 R_{eff}}$	Lactose monohydrate	56/10	Distilled water	

Table 0-1 Summary of drop penetration time models available in the literature.

2.3.Granule formation mechanism

for drop impact granulation, the granule formation mechanism is another significant aspect that will affect the granulation processing and the properties of the granules. Recently, the formation process and mechanisms have been studied for liquid drop impact onto hydrophilic powders, hydrophobic powders, heterogeneous mixtures, and on some natural powders such as sands and minerals [11,12,23–27,15–22]. Emady et al. identified three granule formation mechanisms: Tunneling, Spreading and Crater formation [20,21], which are illustrated in Fig. 2.3. In Tunneling, after the droplet hits the powder bed, it keeps its original shape during nucleation. Here, the nucleus has a strong spherical core with protrusions on the surface. Tunneling was observed for very fine and cohesive powders, and it produced spherical granules. In Spreading, when the droplet impacts the powder bed, it elastically deforms, spreading on the powder surface, and creates a shallow crater. The Spreading mechanism occurs when the drop height is low, and the powder is coarse and less cohesive, producing flat disk granules. With the same coarse powder and a high drop height, when the droplet impacts the powder bed, due to the high momentum of the droplet, it will form a deeper crater with a large diameter, which is the Crater formation mechanism.
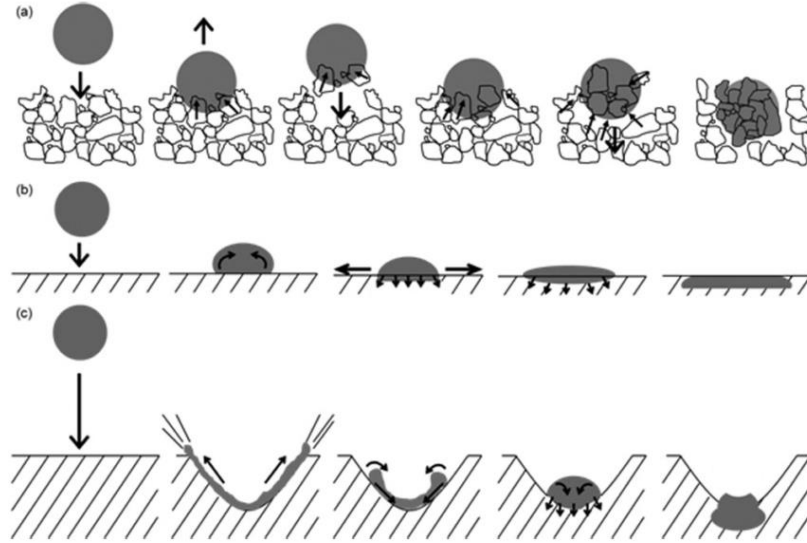
Figure 0.3 Schematics of the three granule formation mechanisms: (a) Tunneling, (b) Spreading, and (c) Crater formation [20].

Furthermore, a regime map of the formation mechanisms was also established [20] in which the formation mechanisms can be distinguished by the granular Bond number, defined as:

$$Bo_g^* = \frac{\gamma cos\theta}{d_{32}^2 \rho_p g} \qquad (9)$$

where γ is the surface tension, θ is the contact angle, d_{32} is the surface mean particle diameter, ρ_p is the apparent particle density, and g is gravity. The granular Bond number, Bo_g^*, is the ratio of the capillary force applied on a particle to the gravitational force applied on the particle. Here, the surface mean particle size was found to be a major factor in influencing the Bond number. It was found that both the bed porosity and the Bond number were the key factors that determined the formation mechanisms. Spreading and Crater formation occurred when $Bo_g^* < 65,000$ for all bed porosities below the fluidization

boundary. The Reynolds number, *Re*, and Weber number, *We,* in this regime affected the granule shapes, and the boundary between Spreading and Crater formation was determined by *We*. In the Spreading regime, where the drop was released at a low height (0.5 cm) with smaller *Re* and *We*, the granules formed were flat disk-like, while in the Crater formation regime, where the drop was released from a higher height (30 cm) with larger *Re* and *We* (*We* ≥ 33), the granules formed were rounder. Tunneling occurred when Bo_g^* >65,000 for all bed porosities. Sphere-like granules were produced, regardless of any liquid properties and drop heights. The granule formation mechanism regime map is shown in Fig. 2.4.
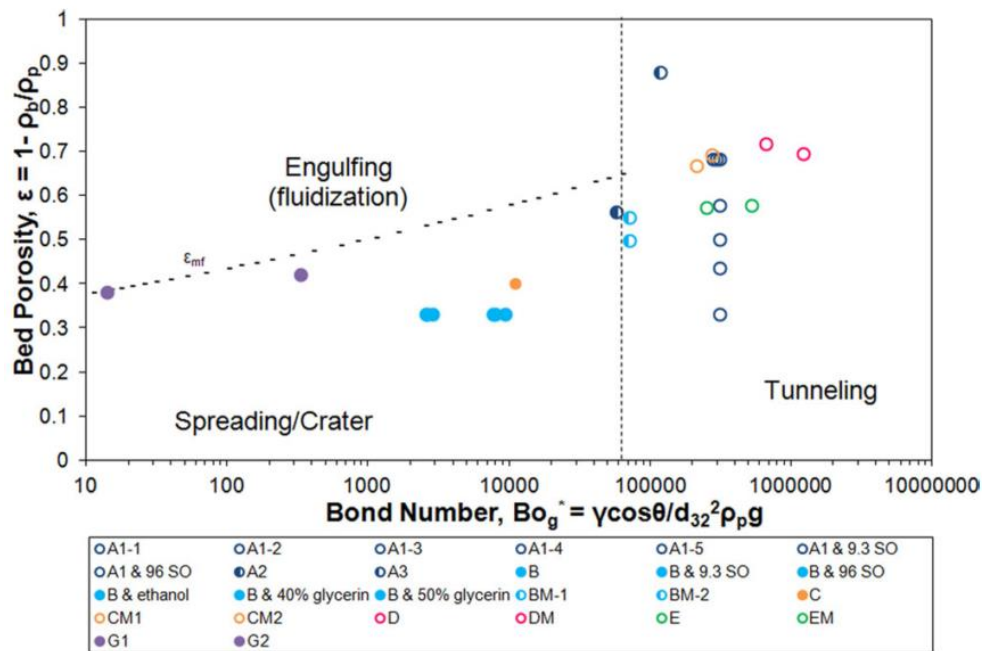
Figure 0.4 Granule formation mechanism regime map [20].

Research on granulation of hydrophobic and heterogeneous (mixtures of hydrophilic and hydrophobic) powders recognized that marble formation occurred on the surface of the liquid droplet during penetration, where small particles spread over and finally covered the

surface of the drop [11,12,17–19]. In their findings, both the liquid surface tension and the impact kinetics were found to be factors that described the formation dynamics of the marble. Hapgood et al. [19] conducted a very comprehensive study on the granulation behavior of hydrophobic powders. They summarized several possible factors from the literature that can explain the powder motion around the liquid drop, among which the "solid-spreading nucleation" is the most common, where hydrophobic powder will spread over the surface of a large drop, corresponding to the marble formation phenomenon. After drying the liquid marble by removing the interstitial liquid, a spherical and hollow granule is formed. Four size grades of glass ballotini and two hydrophobic powders, salicylic acid and 2-Ethoxybenzamide, were used to perform single drop experiments with five different liquids. Based on their findings, several steps must occur to guarantee the formation of a liquid marble and spherical hollow granule. In summary, smaller particle sizes, lower fluid viscosities, and higher kinetic energies during impact favored the marble formation. Whitby et al. [11,12] investigated the effects of liquid properties and particle size on agglomeration of hydrophobic powders. Glass beads with three different sizes, coal dust, and molybdenite powder were used as powder substrates, while alcohol-water solutions were used as liquid binders. Those powder-liquid systems provided a range of particle sizes (glass beads: 42±4, 98±8 and 165±15 µm; coal: 90-106 µm; molybdenite: 1-20 µm), shapes, and wettabilities. The contact angles of the particles with the liquid drops were manipulated by varying the liquid surface tension. At low surface tension of the liquid with

14

a smaller contact angle, the drop penetrated into the powder bed. At high surface tension, marble formation occurred by the particles coating the drop surface. Particle size also had a significant effect. As shown in Fig. 2.5, larger particles (100 μm), encapsulate the droplet, forming a close-packed layer. on the other hand, the droplet can be coated by fine particles (about 10 μm) during the bouncing and rolling on the bed, before coming to rest (see Fig. 2.6). This is a typical coating mechanism of marble formation of a drop on hydrophobic pharmaceutical powders.
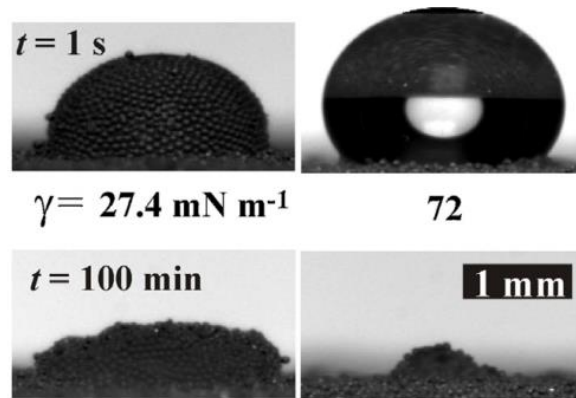
Figure 0.5 Droplet (V= 10 μl) appearance at the indicated surface tensions after 1 s (top) and 100 min (bottom) after impacting powder beds of hydrophobic glass beads (98±8 μm). The black scale bar corresponds to 1 mm [12].
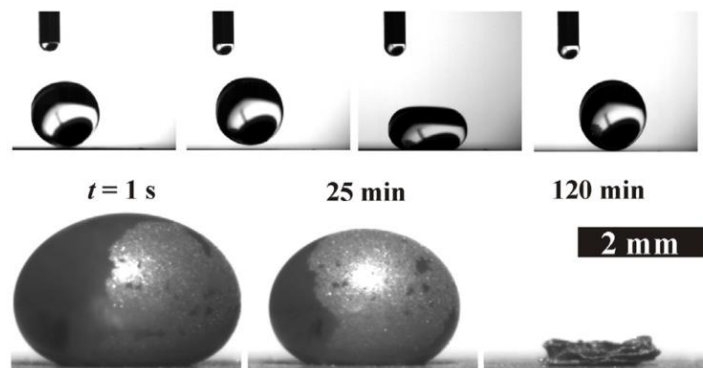
Figure 0.6 Water droplet rolling on the packed beds of molybdenite particles (10 μm in diameter) (top). Water droplet appearance at different times after it came to rest (bottom). The black scale bar corresponds to 2 mm[12].

Kumar et al. [18] explored the granulation of a droplet onto microporous particles. Three different types of particles (Cycas revoluta (sago), Papaver somniferum (poppy), and Sinapis alba (mustard)) were investigated. The poppy and mustard particles have water repellency, while the sago particles are more hydrophilic, due to their different micro patterns, which are represented by the FESEM images in Fig. 2.7. Sodium dodecyl sulfate (SDS) and glycerol were mixed to study the effects of surface tension and viscosity. Single drop experiments were performed on each particle type and also on heterogeneous mixtures. A high surface energy droplet would form a temporary stable marble on a high porosity bed such as poppy, as shown in Row I, Fig. 2.8, where poppy particles were pinned onto the droplet surface. A permanent stable droplet was formed on the bed of mustard particles, as shown in Row II, Fig. 2.8, where the weight of the particles was too heavy to be pulled upward by the surface tension force against the gravity. Increasing the viscosity of the droplet resulted in a Wenzel stable lens, which stays statically on the bed surface and pins the contact angle, delaying the marble formation. Hydrophilic sago particles and crushed sago particles embedded inside the droplet surface instead of encapsulating on the surface, as shown in Rows III and IV, respectively (see Fig. 2.8). Heterogeneous beds composed of poppy and sago particles showed two types of marble formation on different sides of the droplet.

16
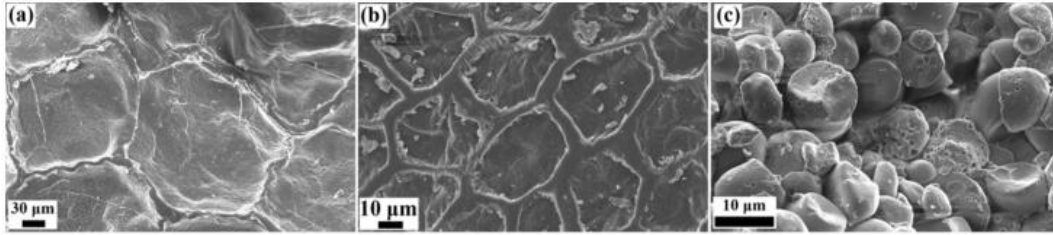
Figure 0.7   Field enhanced scanning electron micrographs (FESEM) of the surfaces of: (a) Papaver somniferum (poppy), (b) Sinapis alba (mustard), and (c) Cycas revoluta (sago)[18].
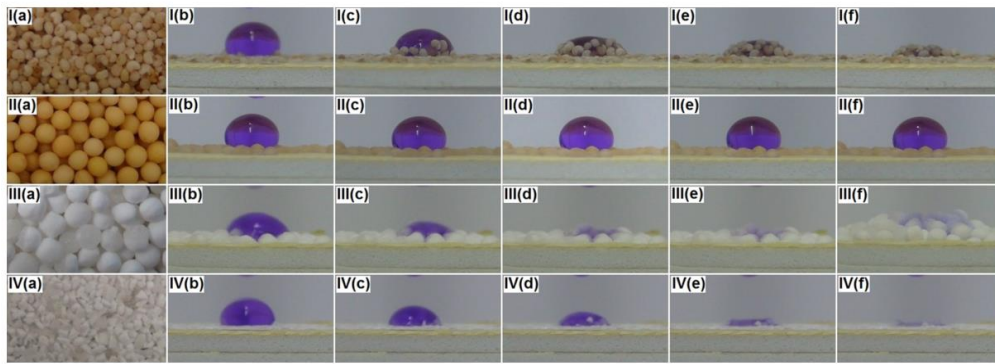
Figure 0.8 Dynamics of a water droplet on porous-granular beds composed of poppy particles (bed void fraction, $\phi = 0.39$) in row I, mustard particles ($\phi = 0.43$) in row II, sago particles ($\phi = 0.47$) in row III, and crushed sago particles ($\phi = 0.57$) in row IV. Image (a) in each row shows the bed morphology before the droplet was dispensed. Images (b−f) show the permeation of the droplet with time, t. I(b)−I(f) correspond to t = 0, 20, 40, 60, and 80 s; II(b)−II(f) correspond to t = 0, 10, 20, 30, and 100 s; III(b)−III(f) correspond to t = 0, 0.04, 0.08, 0.12, and 1.6 sand 0.24 s [18].

The granule formation mechanisms based on the particle and liquid properties from the literature are summarized in Table 2.2.

formation mechanism	Particle and liquid properties	Reference
Tunneling	Very fine and cohesive, bond number >65000	[20]
Spreading	Coarse and less cohesive, bond number <65000	
Crater formation	Coarse powder, high *We* and *Re*	

Solid-spreading nucleation/marble formation	Smaller particle size, lower fluid viscosity, and higher kinetic energy	[19]
Drop penetration	Large particles (100 μm), small contact angle	[11,12]
Marble formation	Fine particles (10 μm), large contact angle	
Wenzel stable lens	Heavy hydrophobic particles (1.68 mm), high surface energy droplet	[18]
Marble formation	Small hydrophobic particles (0.94 mm), high surface energy droplet	
Powder permeation	Small hydrophilic particles	

Table 0-2 Summary of granule formation mechanisms available in the literature.

2.4. Single drop impact onto soil and sands

In addition to the study on fine powders for various manufacturing processes, single drop impact experiments are also applied to soil and sand to mimic the raindrops splashing onto the ground. This phenomenon is relevant to some important natural and industrial processes like soil wetting and field irrigation. Xiang Cheng's group [22,23,25] and Devaraj van der Meer's group [16,24,26,28] mainly focus on the liquid-solid impact studies that are analogical to the condition of raindrop impact.

Zhao et al. [22] investigated the granular impact cratering formed by liquid drops on soda-lime glass beads with a particle size of 90 ± 15 μm. They revealed the liquid drop-impact dynamics by studying the morphology of impact craters and also compared it with the Schmidt–Holsapple (S-H) scaling rule in asteroid strikes. The crater diameter, D_c, has a power-law with 0.17 scaling which is quantitatively similar to S-H scaling. A similar study was conducted by the same group, where Zhang et al. [23] studied the scaling of

18

liquid-solid impact on both dry and wet granular material. They set up different water saturation levels in the powder bed up to 1% and found that the dynamics and the morphologies of the impact cratering in wet granular material are quantitatively different from that in dry granular media. The crater diameter, D_c, is a function of impact energy, E, and the size of the impinging drop, D_d, with a power-law scaling, $D_c \sim E^\beta D_d^\gamma$, where β is the power-law exponent with different values in higher saturation beds, and γ changes from 1/3 scaling for a dry powder bed to 2/5 scaling for a wet powder bed.

Zhao et al. [26] studied the dependence of the dynamics of the granular media on impact energy and packing fraction. They discussed both the deformation of the granular substrate and the droplet. Based on their findings, the deformation of the granular substrate decreased with the increase in the initial packing fraction. However, they defined a critical packing fraction, $\varphi^*=0.585$, to which the powders were rearranged during the impact, independent of the initial packing fraction. The droplet maximum deformation, D_d^*, followed a scaling law, $D_d^* \sim We^{*1/4}$, where We^* is the effective Weber number, which can explain the morphology transition between three different observed crater shapes. Another paper from Zhao et al. [16] reported the effects of the wettability of grains and the grain size on the impact dynamics. Three granular materials were used: silane-coated soda-lime (with grain size $d = 114$ and 200 μm, and contact angle with water $cos\theta < 0$), ceramic (grain size $d = 98$, 167 and 257 μm, $cos\theta = 0.3$) and pranha-cleaned ceramic (grain size $d = 98$, 167 and 257 μm, $cos\theta = 0.6$-0.7). for large grain sizes ($d\sim257$ μm), the droplet spreading was

stopped by the liquid-grain mixing rather than the surface tension; hence, it was governed

by the effective Reynolds number, $Re*$, according to the relation $D_m/D_0 \propto Re*^{1/5}$, where D_m

is the maximum spreading diameter and D_0 is the droplet diameter. for small grain sizes

(d~98 μm), the mixing was slower and the surface tension balanced the inertia, where the

effective Weber number governed the spreading, according to the relation $D_m/D_0 \propto We*^{1/4}$.

With the increase of the grain wettability, the maximum droplet spreading transitioned

from a capillary regime to a viscous regime.

2.5.Granule characterization

Key characteristics of the granules include their morphology, microstructure and

content uniformity.

2.5.1. Granule morphology

The morphologies of the granules made from single drop granulation are affected by

several parameters, such as particle size distribution, particle wettability, liquid surface

tension, and impact velocity [8,20,21]. Emady et al. [21] investigated the granule

morphology from single drop granulation and categorized the shape and size based on the

formation mechanisms. The shape and size of the granules were indicated by the horizontal

aspect ratio, H.A.R. (d_{max}/d_{min}), and the vertical aspect ratio, V.A.R. (d_a/h_{max}), where d_a is

the projected area equivalent diameter, h_{max} is the maximum granule height, and d_{max} and

20

d_{min} are the maximum and minimum granule diameter, respectively. Typically, the granules formed via Tunneling were nearly round, with V.A.R. = 1.05-1.10 from loosely-packed beds. Granules formed via Spreading were flat disks, with V.A.R. = 2.33-2.73, and when switching the binder from water to silicone oil, both V.A.R and granule size increase. In this case, the V.A.R values are much larger than the H.A.R. values, which can only indicate the circularity from its top view. Thus, the V.A.R values were a better characterization of the granule roundness. Granules formed via Crater formation were mushroom-like and rounder (V.A.R. = 1.22-2.47), compared with those from Spreading. Also, granules produced using water were much rounder than those formed using silicone oil. Emady et al. [20] also extended the investigation on granule morphology to a wider variety of powder materials. In the Spreading and Crater formation regimes, the granule shape was affected by liquid properties, drop size and drop height (factors in *Re* and *We*). In Spreading, granules formed were flat disks, while in Crater formation, with decreasing *We*, granules were rounder. In the Tunneling regime, the granules were round with low V.A.R., and they were insensitive to the factors in *Re* and *We*.

The granule morphology was also found to be affected by the wettability of the powders, based on the work from Emady et al. [8]. for powder mixtures mainly consisting of hydrophilic components, the granules formed were large. The core nucleus was surrounded by a layer of powder. As the amount of hydrophobic components increased in the mixture, the shapes of the granules became more irregular and the size also decreased.

21

2.5.2. Granule internal structure

The pores or voids inside the granule influence some essential performance properties such as strength, homogeneity and dissolution. X-ray computed tomography (XRCT) is a popular technique that has recently been used in granule characterization [29–38], due to its ability to measure the material density and internal structure in a nondestructive and highly accurate way. It can determine the porosity and pore distribution by sets of two-dimensional scanning images and building up a three-dimensional reconstruction by some mathematical treatments.

There are some early studies on granules using XRCT. Farber et al. [29] studied the porosity and pore size by comparing XRCT and mercury porosimetry. Mannitol- and lactose-microcrystalline cellulose-based blends were granulated in low and high shear granulators. Based on the results, the two characterization techniques gave very similar overall porosities, while the pore sizes differed by about two orders of magnitude. The overall porosities of the granules made from the low shear rate were much larger (~58%), compared with those made from the high shear rate (~16%). From the cross-sectional images, the major difference between their structures is not the pore size, but the way they are connected. XRCT is not as accurate as porosimetry in measuring the connected porosity, but on the other hand, it can provide qualitative information on the pore size and spatial distribution of the pores. However, there are measurement limits due to the instrument resolution. Similarly, Rahmanian et al. [31] compared the function of XRCT, Geopyc

(using a highly free-flowing fine dry powder to fill in the interstices of the particle samples), and mercury porosimetry in measuring the granule porosity, as well as the influence of different impeller speeds. The overall granule porosity reduced with higher impeller tip speed, from 38.6% to 16.7%, when the speed increased from 230 to 350 rpm. Granules made from higher speeds were more heterogeneous, where the particle size distributions were wider. The values from different measuring techniques also varied. The calculated porosities from XRCT were higher than those from the Geopyc and mercury porosimetry.

The effect of powder hydrophobicity on granule internal structure was investigated by Hapgood et al. [30] via XRCT. A formulation with a high proportion of the hydrophobic ingredient (~70%) was used in both single drop and high shear granulation. The tomographic images of the granules from different sieve fractions showed that most of the finer granules were consolidated and had a small empty core, while the larger granules had multiple hollow nuclei that were surrounded by a thick homogenous powder shell. The results were consistent with the solid spreading nucleation mechanism that occurred during liquid marble formation with highly hydrophobic powders.

XRCT has also been applied in pharmaceutical granulation. Kašpar et al. [33] investigated the internal structure as well as the dissolution of acetaminophen from granules formed via high shear granulation. The granules were made from two powder ingredients: acetaminophen, as the active pharmaceutical ingredient (API), and Avicel PH-200 (microcrystalline cellulose), as the excipient. A factorial design was made in terms of

three variables: L/S ratio, impeller speed and wet massing time. The results of the XRCT analysis showed that the internal structure and the porosity significantly depend on the process variables. The measurement of the porosity after the dissolution of acetaminophen indicated that it was uniformly distributed throughout the granule internal volume for all processing cases. This means that there was no preferential accumulation of the API or preferential wetting of the excipient. Dale et al. [34] investigated the granule phase volume distribution using XRCT, where the spatial distribution of particles, binder and air volumes were segmented. Granules were made through single drop granulation on glass ballotini particles (d = 250-335 μm) by an aqueous solution of 0.15 g/g of polyvinylpyrrolidone (PVP) in DI water. Phase volumes were differentiated by a combination of gray intensity value thresholds and image processing. Glass beads are insensitive to the gray volume thresholds, while the PVP is sensitive to lower gray value thresholds. Thus, the segmentation can be reflected from the image analysis. Based on the results of axial phase distributions, the tops of the granules had larger air volume fractions than the centers and bottoms of the granules, due to the concaves on the tops that formed during the drop penetration. In the granule body, the particle volume fraction ranged from 62-64% while the air volume fraction was 32-35%, and the volume fraction of binder was less than 5%. Binder volume was preferentially distributed on the tops of the granules, which should result from the gradient formed during the percolation of the drop.

Besides granulation from large particle sizes (hundred μm scale), the microstructures of granules made from ultra-fine powders were also studied by Davis et al. [37]. α-Alumina particles with particle sizes of 0.5 μm (Powder A), 5 μm (Powder B), 25 μm (Powder C), and 108 μm (Powder D) were used in single drop granulation by an aqueous PVP solution. Powder beds were prepared by sieving the alumina particles into a petri dish using 1.4 mm, 710 μm and 500 μm sieves. The XRCT images show a significant effect of particle size on the granule internal structure (see Fig. 2.9). There are large, discrete voids surrounded by dense particles in Powder A granules, while Powder B granules have a few void spaces. Powder C granules have some large cracks and a diffuse pore network in the granule body, while Powder D granules have a pore network that was formed by hollow aggregates. The macro-voids volume fraction of the total granule is also affected by the particle size. Decreasing the particle size will increase the macro-void volume. Besides the primary particle size, there is also a significant effect of the bed preparation on the internal structure of Powder A granules. Granules from A1 (Powder A sieved through a 1.4 mm sieve) have larger macro-voids than those in the granules from A2 (sieved through a 710 μm sieve) and A3 (sieved through a 500 μm sieve). on the other hand, the effect of bed preparation on the structures of granules from Powder B is weaker compared with Powder A, while there is almost no effect for Powders C and D.
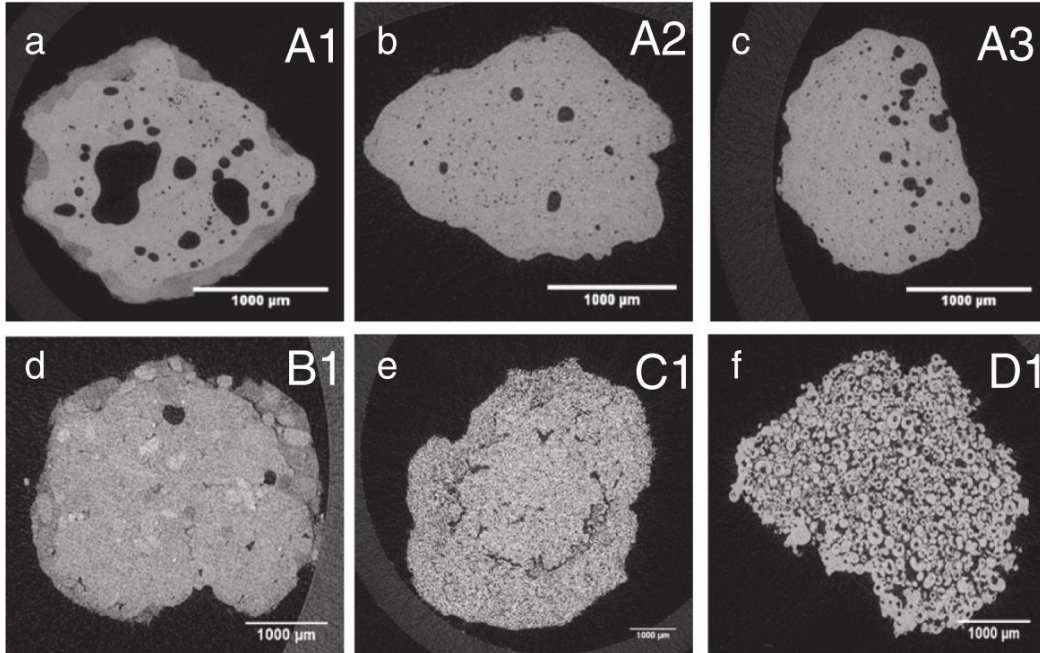
Figure 0.9 Representative XRCT slices of the granules made from: (a) Powder A1, (b) Powder A2, (c) Powder A3, (d) Power B1, (e) Powder C1, and (f) Powder D1, (1: powder sieved through 1.4 mm sieve, 2: powder sieved though 710 μm sieve, 3: powder sieved through 500 μm sieve) [37].

2.5.3.   Content uniformity

In addition to the aforementioned granule properties in the previous sections, the content homogeneity is also of significant importance in wet granulation, especially in the pharmaceutical industry. The granule content homogeneity has been studied in single drop, high shear and continuous granulation [39–48] to investigate the effects of the formulation properties as well as the granulation process parameters. Among them, the hydrophobicity and primary particle size of the ingredients are considered crucial factors that influence the content uniformity distribution across the granule size classes.

26

Nguyen et al. [40] investigated the effect of hydrophobicity on drug uniformity of a salicylic acid and lactose mixture in high shear granulation. As was the case with the binder of PolyVinylPyrrolidone (PVP) solution, where the wettability between powder and binder was good, the drug distribution was homogeneous across all granule size fractions. In contrast, when water was used as the binder, the granule compositions were compromised (the actual API amounts were lower than theoretically expected). The intermediate granule size fractions were deficient of drug content, while the finest and coarsest size fractions were enriched with drug content. This can be attributed to the preferential wetting of the hydrophilic ingredients that causes the overall preferential granulation of these components. Similarly, Oka et al. [42] investigated the effects of improper mixing and preferential wetting of two particulate components (MCC, APAP) on content uniformity in high shear granulation. Both the powder mixture before the granulation and the granules formed after granulation were sampled. It was found that during the dry mixing stage, the top layer of the powder bed was sub-potent of the API compared with the theoretical value, indicating a potential cause of non-uniformity. for granule content uniformity, fine granules were super-potent with API, while the coarse ones were sub-potent. A fraction of APAP remained ungranulated, likely due to the fact that MCC has a lower contact angle and thus a higher wettability with water compared with APAP, thus creating large disparities across all granule sizes. To further analyze the origin of the non-uniformity, additional work was carried out by Oka et al. [41] to compare the product content uniformities from both single

27

drop granulation and high shear granulation. They found that for a low API load (3-20 %), the main cause of content non-uniformity may not be the preferential wetting of one component with the binder, but rather a combination of particle segregation during the dry mixing stage and the different kinetics of the granulation rate processes.

2.6. Summary of the literature and significance of the work

In single drop granulation, drop penetration time measurement and formation mechanisms investigation have been done for mono- and multi-component particle systems. However, the drop penetration time for granulation on multi-components, especially those containing hydrophobic parts, still deviate from the models. Additionally, there are disagreements on formation mechanisms for single drop granulation on heterogeneous powder mixtures, and there is a lack of investigation into pharmaceutical particles.

Little work has been done to relate the granule properties, like morphology, internal structure, and content uniformity to the granule formation mechanisms and formulation properties. Also, most of the work has only focused on homogenous particles. The properties of granules (beyond size distribution) formed from heterogeneous mixtures from either single drop granulation or high shear granulation have received little attention.

In this dissertation, I will investigate the single drop granulation of mixtures of two kinds of pharmaceutical particles, with different particle sizes and contact angles with water, to understand the relationships between drop penetration time and formation mechanisms and particle and liquid properties on the resulting granule attributes. In addition to granule size distribution, the granule morphology, internal structure and content uniformity will also be investigated. A regime map for single drop granulation of mixtures is also established to predict and optimize the granulation process for these complex materials.

CHAPTER 3. MATERIALS CHARACTERIZATION AND EXPERIMENTAL METHODS

3.1. Introduction

The properties of the powder and liquid used in wet granulation are important to characterize, as they influence the granule formation process as well as the properties of the formed granules. This section will detail the materials used for single drop granulation, the single drop impact experiments performed, as well as the characterization of the granule properties like morphology, internal structure and content uniformity.

3.2. Materials Characterization

3.2.1. Materials used

Micronized acetaminophen (COMPAP® COARSE L, APAP, Mallinckrodt Inc., Raleigh, NC) was used as the API and microcrystalline cellulose (Avicel PH-101, FMC BioPolymer, Philadelphia, PA) was used as the excipient. DI water was used as the liquid binder. All experiments were performed at room temperature.

3.2.2. Particle and liquid characterization

The pure as-received MCC and APAP had coarse surface mean particle sizes (d_{32}) between 30-50 μm. To compare the effects of particle size distribution and contact angle, finer micronized particle sizes of both MCC and APAP were prepared with a jet mill (Model 00 JET-O-Mizer system, Fluid Energy). The particle size was characterized using optical microscopy (Malvern Morphologi G3SE). A volume of 5-7 mm^3 was selected as the test sample and the measurement was carried out by the wet evaporation unit method (using ethanol to disperse the powder), which is appropriate for fine, adhesive particles. The theoretical particle sizes were calculated using the measured surface mean particle sizes (d_{32}) of 100% MCC and 100% APAP. The calculation was based on the percentage of each component in the mixture: $d_{theo} = X_{MCC} d_{MCC} + X_{APAP} d_{APAP}$, where X_{MCC} is the weight fraction of MCC and d_{MCC} is the true particle size of MCC, and similarly for APAP. The true particle density was measured by a helium pycnometer (Micrometrics Accupyc II 1340) and the particle pore volume was measured by a Hg porosimeter (Micromeritics AutoPore IV 9500 Series). The properties of the powder materials are shown in Table 3.1. The apparent density was calculated as $\rho_p = \rho_s/(1 + V_p \rho_s)$. All of the particle properties were measured from three to five replicates.

Materials	MCC	APAP
Coarse d_{32} (μm)	33.7 ± 9.6	46.2 ± 11.0
Fine d_{32} (μm)	15.9 ± 5.1	11.5 ± 2.7
True density ρ_s (g/cm^3)	1.63 ± 0.03	1.29 ± 0.01
Pore volume V_p (cm^3/g)	0.000759	0.000455
Apparent density ρ_p (g/cm^3)	1.63 ± 0.03	1.29 ± 0.01

Table 3-1 Particle Properties

The liquid binder used in wet granulation was distilled water, and the properties are

shown in Table 3.2. The viscosity, density and surface tension were reference values [20].

The drop diameter was measured by releasing the droplets, and 5 replicates were recorded

by a high-speed camera (Photron Fastcam-X 1024 PCI). A ruler was used beside the

syringe to measure the size of the droplet.

Liquid	Viscosity (mPa*s)	Density (g/mL)	Surface tension (mN/m)	Syringe needle gauge	Drop diameter (mm)
Distilled water	1	1	72.0 ± 0.3	22	2.71 ± 0.03

Table 3-2 Liquid Properties

3.2.3. Contact angle

Powder wettability has been studied widely [49,50,59–61,51–58] due to its significant

role in affecting the wet granulation process. The contact angle values with water for pure

MCC and APAP are taken from the literature [42]. A traditional way to calculate the contact angle for heterogeneous mixtures uses Cassie-Baxter theory [62]: $cos\theta = f_1cos\theta_1 + (1-f_1)cos\theta_2$, where f_1 is the mass fraction of MCC and θ_1 and θ_2 are the contact angles of MCC and APAP, respectively. However, Mundozah et al. [61] found it difficult to apply the Cassie-Baxter theory to a binary mixture where the component powders differ in size, and thus revised the theory:

$$\overline{cos\theta^*} = f = \min\left(\frac{1-\emptyset}{1-\emptyset_c} * \frac{\emptyset_c}{\emptyset}, 1\right) \tag{10}$$

where $\emptyset$ is the volume fraction of large particles and $1-\emptyset$ is the volume fraction of small particles. $\emptyset_c$ is the critical value fraction at which larger particles are completely covered by smaller particles, given by:

$$\emptyset_c = \frac{1}{\frac{4d_2}{d_1}+1} \tag{11}$$

where d_1 is the particle size of the larger particles and d_2 is the particle size of the smaller particles. Consequently, Eqn. (10) reveals a non-linear relationship between the contact angle and the powder volume fraction, due to the possibility for the smaller particles to coat the larger particles. $\overline{cos\theta^*}$ is the normalized wetting parameter, which is equal to f, the volume fraction of the larger particles in the powder mixture.

3.3. Experimental Methods

3.3.1. Single Drop Granulation

To investigate the effects of particle size and hydrophobicity on granulation, four different MCC/APAP mixtures were made based on their sizes (as provided in Table 3-1): Coarse-MCC/Fine-APAP, Coarse-MCC/Coarse-APAP, Fine-MCC/Fine-APAP and Fine-MCC/Coarse-APAP.

The initial two-component combination chosen was Coarse-MCC/Fine-APAP. Mixtures of MCC/APAP with weight proportions of 100/0, 90/10, 80/20, 75/25, 70/30, 65/35, 60/40, 50/50, 40/60, 30/70, 20/80, 10/90 and 0/100 were made by measuring the weights of the two components. for the other three mixture combinations (Coarse-MCC/Coarse-APAP, Fine-MCC/Fine-APAP and Fine-MCC/Coarse-APAP), only 90/10, 70/30, 50/50, 30/70 and 10/90 proportions were made.

Each batch was well-mixed with a Turbula Shaker Mixer at 46 rpm for 20 minutes. Each powder mixture was sieved through a 2.00 mm sieve into a Petri dish and then levelled by a stainless-steel spatula to get a smooth surface. The bed density, ρ_{bed}, was calculated by dividing the mass of powder in the Petri dish by the volume of the Petri dish. A 100 µL syringe was filled with liquid binder and held at 5 mm above the powder surface, and a single drop was released from the syringe manually. The granules were excavated by scooping them out individually by a spatula.

34

A high-speed camera (Photron Fastcam-X 1024 PCI) was used to record the granule formation process. for batches of MCC/APAP resulting in the Spreading formation mechanisms, since there is not very much powder covering the droplet during the penetration, it is easy to tell when the droplet completely penetrates into the surface of the powder bed. Yet, after the penetration, the surface of that spot is still shining, indicating that water is still penetrating into the powder bed. This phenomenon provided motivation to measure the penetration time twice: the first is the time when the droplet completely sinks into the powder bed, and the second is the disappearance of the shining. However, for single drop granulation on batches resulting in the Tunneling mechanism, since the smaller particle size dominates, the penetration time increased tremendously. Here, the droplet will not penetrate completely into the powder bed, but will sink down to a certain level. Thus, for these batches, only one penetration time is measured: the time when the sinking stops. Six replicates were performed for each batch.

3.3.2. Crater Diameter Increase

To visually determine the transition of the formation mechanism between Tunneling and Spreading, pictures of a crater diameter increase captured by the high-speed camera were taken. These pictures were used to compare the diameter of the crater when the droplet impacts the powder bed to the diameter of the crater when penetration completely stops. Using Image J, this change in crater diameter was measured as the crater diameter increase.

3.3.3. Granule Morphology

The granule morphology was characterized using a prism setup and vertical camera [21]. for each batch, 6-8 granules were excavated by scooping the granules out individually using a spatula. The granules were placed next to the prism to capture the top and side views simultaneuously. ImageJ was used to analyze the images to measure the projected area equivalent diameter (d_a), maximum granule height (h_{max}), maximum diameter (d_{max}), and minimum diameter (d_{min}). From these measurements, the horizontal aspect ratio, H.A.R. (d_{max}/d_{min}), and the vertical aspect ratio, V.A.R. (d_a/h_{max}), were calculated.

3.3.4. Granule Surface Structure

The microstructures of the granule surfaces were examined by scanning electron microscopy (SEM) (Amray 1910 Field Emission Scanning Electron Microscope). The samples were pre-coated with a gold layer (Au sputter coater) before the measurement, since both MCC and APAP are non-electro-conductive.

3.3.5. Granule and Bed Packing Internal Structure

The internal structures of the granules and bed packing were characterized using a micro-CT system (ZEISS Xradia 502 Versa, Carl Zeiss X-ray Microscopy Inc., Pleasanton,

36

CA, US), housed in the Center for 4D Materials Science at Arizona State University. A sealed transmission source emits X-rays through the sample seated on an ultra-high precision rotation stage, which was rotated within the entire range of 0-360° with a step angle of 0.11°, resulting in 3601 radiographs. The projected image then impinges on a scintillator, which converts X-rays to visible light, and is subsequently magnified by an optical objective lens before reaching the 2048 x 2048 pixel charge-coupled detector. Granules made from pure MCC, pure APAP, 70 % MCC and 90 % MCC were scanned in the micro-CT. In order to obtain images with sufficient contrast and resolution from which the structural constituents can be easily separated, the X-ray source settings (tube voltage and current), physical imaging setup parameters (like source to sample distance and sample to detector distance) and exposure time were adjusted for each granule while obtaining the optimal voxel size achievable. The X-ray projections were processed for noise reduction using a Gaussian filter, before being reconstructed using Xradia XM-Reconstructor software with a correction for beam hardening and centre of rotation.

Reconstructed data in the form of TIFF files were then imported into Avizo (Version 9.0, FEI Visualization Sciences Group) for further image processing. A diffusion-based smoothing filter (Non-Local means) followed by a sharpening filter (Unsharp masking) was used to reduce noise, reinforce the contrast at the edges, and make details appear sharper in the datasets. Then, segmentation (binarization) was performed for separating the pixels of the grayscale images into background and foreground, i.e., voids and particles.

Although the same image processing steps were applied for each granule volume, individual tailoring of thresholding values was required.

After the completion of image processing, the internal microstructure of granules was studied. Quantitative analysis of calculating the porosity was performed on these binary images using an in-built Avizo analysis module (volume fraction) by considering sub-volumes contained fully inside the granule at different coordinates, which is illustrated in Figure 3.1. for pure MCC granules, a total of 8 sub-regions were chosen from two MCC samples (5 from sample 1 and 3 from sample 2). for pure APAP granules, a total of 12 sub-regions were chosen from two samples (5 from sample 1 and 7 from sample 2). for 70 % MCC granules, a total of 12 sub-regions were chosen from two samples (7 from sample 1 and 5 from sample 2). only three sub-regions were selected in the 90 % MCC granule, since very consistent porosities were observed.
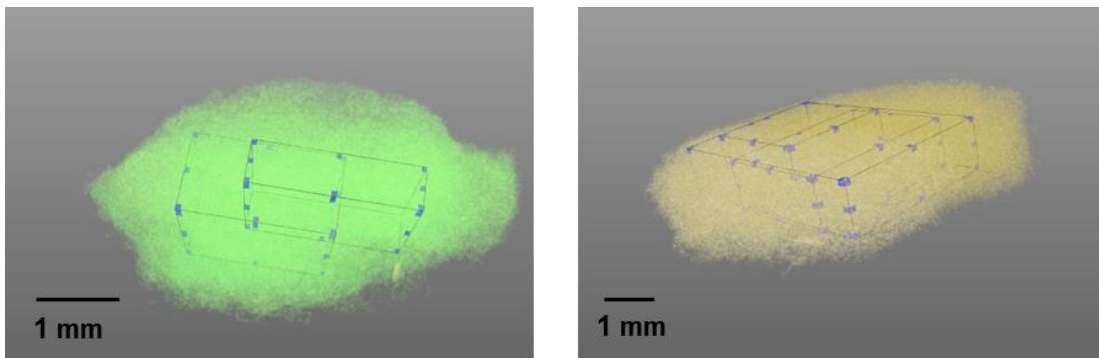
Figure 3.1 Illustration of sub-volumes chosen in 70% MCC (left) and pure MCC (right) granules. Volume renderings of granules are made partially transparent for better visualization.

A mixture from Coarse-MCC/Fine-APAP with 30 % APAP was selected for investigating the powder bed packing structure. It would be a time intensive process to scan the entire powder bed with a duplicate (in our case, a volume of 350 mm^3 would be scanned in approximately 15 hours). Hence, sampling random areas was resorted to, and care was taken to avoid any artificial changes to the microstructure of the sample. To prepare the intact sample of powder bed packing, two 1.5 mL microcentrifuge tubes were cut from the tip end and then tapped onto two random areas that were relatively far apart within the petri dish. Following the method in Section 3.3.1, after filling the petri dish with the powder mixture, two tubes were filled with powder (see Fig 3.2) and then carefully moved from the petri dish and sent for micro-CT scans.
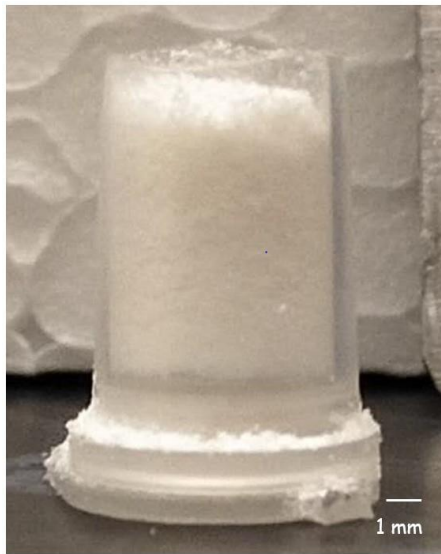
Figure 3.2 Photo of powder packing column sample of 30 % APAP in a Coarse-MCC/Fine-APAP mixture.

3.3.6. Content Uniformity

In order to investigate the bed homogeneity of the MCC-APAP system, powder mixtures from the petri dish were sampled at 5 randomly chosen positions. The same as Chapter 3.3.1, for Coarse-MCC/Fine-APAP mixtures, batch proportions of 90/10, 80/20, 75/25, 70/30, 60/40, 50/50, 30/70, 20/80 and 10/90 were tested. for the other three mixture types, only proportions of 90/10, 80/20, 50/50, 30/70 and 10/90 were tested. for content from the powder bed, samples were carefully extracted by a spatula from the surface of the powder bed, with about 5 mm depth, with the weight of each sample between 20 and 50 mg, based on the weight of the granules formed and the formation mechanism. The spatula was wiped clean before extracting the next sample to prevent any contamination from the previous sample. The scooped powder was stored in a centrifuge tube.

UV-vis spectrometry (Evolution 200 series, Thermo Fisher Scientific) was used for determining the amount of acetaminophen in the bed surface and granules. Acetaminophen is soluble in absolute ethanol, while microcrystalline cellulose is not. for content in the granules, a pre-weighed amount of granules (four to six granules, with each granule weighing from 20 mg to 60 mg, based on an approximation of APAP concentration) was measured for each trial, and a total of six trials were performed for each mixture proportion. Both the bed surface samples and granules were incubated in 10 mL ethanol overnight on a shaking platform and kept out of light (APAP is sensitive to UV light). 10 μL of the

solution was extracted and added to 3 mL of pure ethanol in a cuvette [42]. The absorbance was measured at a wavelength of 250 nm, where the extinction coefficient of the acetaminophen in ethanol is 12896 L mol^{-1}* cm^{-1} (measured by calibration experiments). The measured APAP content was then compared with the theoretical value in each proportion to assess the content uniformity.

CHAPTER 4. MECHANISMS OF SINGLE DROP GRANULATION ON HETEROGENEOUS POWDER BEDS

4.1.Introduction

In this chapter, single drop granulation on heterogeneous powder mixtures of microcrystalline cellulose (MCC) and micronized acetaminophen (APAP) will be performed. The drop penetration times and granule formation mechanisms will be examined using high-speed video. Additionally, the resulting granule morphology will also be analyzed. The results will provide an understanding of how the formulation properties and granulation process affect the single drop penetration and granule properties.

4.2.Drop Penetration Time and Granule formation Mechanisms

4.2.1. Coarse-MCC/Fine-APAP Mixtures

The drop penetration time results of single drop granulation on Coarse-MCC/Fine-APAP mixtures are shown in Fig. 4.1 and Fig 4.2. for batches from 100/0 to 60/40, both the first and second penetration time are increasing with the increase of the percentage of APAP, within experimental deviation. for batches from 50/50 to 0/100, the drop penetration becomes extremely slow, and the Tunneling mechanism dominates. The second penetration time is hard to measure, so the first penetration time is chosen as the

only penetration time for those batches. Generally, the penetration time increases with the increase of the percentage of APAP, but the time for 0/100 is shorter than that of 10/90. This may also be due to the improper mixing of the powders, as was seen with the 65/35 batch. Since the particle size of APAP is much smaller than that of MCC, these particles are likely to form aggregates. This will cause the powder bed to exhibit different local packing properties like bed density and porosity. When a drop impacts onto the bed with different local variations, it will affect the penetration time.
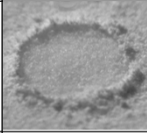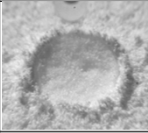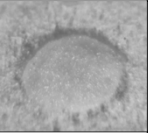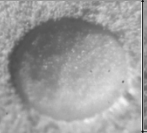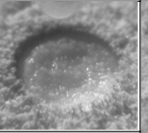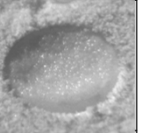
MCC/APAP	100/0	90/10	80/20	75/25	70/30	65/35
D[3,2] (Surface mean) (μm)	54.8±14.8	49.6±11.6	33.2±6.73	29.6±6.42	29.2 ±5.92	22.89±4.78
Theoretical mean particle size d_{theo} (μm)	54.82	50.31	45.80	43.55	41.29	39.05
Bed density ρ_{bed} (g/cm^3)	0.298	0.251	0.244	0.210	0.237	0.202
First penetration time t_1 (s)	0.0998±0.00455	0.0868±0.00444	0.160±0.0081	0.252±0.0173	0.504±0.00895	0.503±0.0418
Second penetration time t_2(s)	0.114±0.00498	0.119 ±0.0082	0.219±0.0201	0.655±0.0823	0.786±0.0213	0.975±0.262
Finalized penetration						
Estimated formation mechanism/ Crater diameter increase d_c(mm)	Spreading/ 1.47 ±0.12	Spreading/ 1.23 ±0.36	Spreading/ 0.73 ±0.23	Spreading/ Tunneling/ 0.48 ±0.08	Spreading/ Tunneling/ 0.42 ±0.11	Spreading/ Tunneling/ 0.39 ±0.08
Contact angle θ (°)	36	43.1	49.5	52.3	55.1	57.9

Figure 4.1 Single drop granulation results for 100/0 to 65/35 batches of Coarse-MCC/Fine-APAP mixtures.
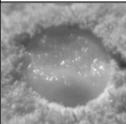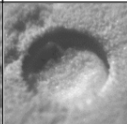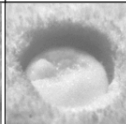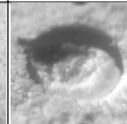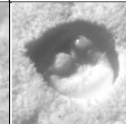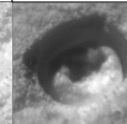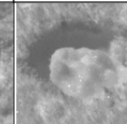
MCC/APAP	60/40	50/50	40/60	30/70	20/80	10/90	0/100
D[3,2] (Surface mean) (μm)	20.75±4.31	26.46±6.15	22.35±6.16	17.45±4.23	12.72±3.56	12.94±3.15	9.74±2.21
Theoretical mean particle size d_{theo} (μm)	36.78	32.28	27.77	23.26	18.76	14.25	9.74
Bed density ρ_{bed} (g/cm³)	0.198	0.177	0.165	0.147	0.131	0.125	0.151
First penetration time t_1 (s)	0.869±0.117	18.02±0.13 (min)	21.45±1.33 (min)	21.38±6.39 (min)	30.69±3.06 (min)	36.14±4.35 (min)	31.99±2.93 (min)
Second penetration time t_2(s)	1.573±0.147	N/A	N/A	N/A	N/A	N/A	N/A
Finalized penetration							
Estimated formation mechanism/ Crater diameter increase d_c(mm)	Spreading/ Tunneling/ 0.28±0.1	Tunneling	Tunneling	Tunneling	Tunneling	Tunneling	Tunneling
Contact angle θ (°)	60.5	65.6	70.5	75.2	79.9	84.5	89

Figure 4.2. Single drop penetration results for 60/40 to 0/100 batches of Coarse-MCC/Fine-APAP mixtures.

for granulation on mixtures of Coarse-MCC/Fine-APAP, by evaluating the formation mechanism of each batch, it is obvious that Spreading occurs in batches of 100/0, 90/10 and 80/20 MCC/APAP. From the 70/30 batch, some characteristics of Tunneling start to occur. We expect the transition point to lie somewhere between the batches of 80/20, 70/30 and 60/40. To determine this transition, small intermediate mixture increments were made: batches 75/25 and 65/35. Additionally, the crater diameter increase that occurs when comparing the diameter from the droplet completely touching the powder bed to the crater diameter when the penetration completely stops is also a good indicator of the formation mechanism. The crater diameter increase should be very obvious in Spreading, while the increase in Tunneling should be minimal. In the batch of 100/0, the diameter increase with

44

the initial diameter can reach up to 42.5%, which is definitely indicative of Spreading. However, it drops down to only 6.2% for the batch of 60/40, so Spreading occurs to a much lesser extent here. The formation mechanism for batches of 75/25, 70/30, 65/35 and 60/40 is considered as Spreading/Tunneling, meaning that the behavior exhibited has characteristics of both mechanisms. for batches with APAP higher than 60%, there is almost no crater diameter change that can be recognized, indicating pure Tunneling.

4.2.2. Coarse-MCC/Coarse-APAP Mixtures

for granulation on mixtures of Coarse-MCC/Coarse-APAP, the formation mechanisms are shown in the image sequences in Fig. 4.3. Different from Coarse-MCC/Fine-APAP, this mixture combination exhibits the Spreading mechanism for all MCC/APAP proportions. An initial hypothesis based on this is that increasing the overall particle size of the bed mixture results in the Spreading mechanism, regardless of the APAP proportion. To further investigate the details of the granule formation, the crater diameter increase from initial impact to final penetration was compared for each mixture proportion (see Fig. 4.4). The average crater diameter increase ranges from 35.8 % to 38.1 %, which are all large enough to indicate the Spreading mechanism, based on the results from Coarse-MCC/Fine-APAP mixtures [63], where Spreading occurred with a crater diameter increase larger than 20 %. Additionally, with higher APAP proportions (above 70 %), marble formation also

occurred (see Fig. 4.3b) [11,18], where the more hydrophobic powders climbed onto and covered the liquid droplet once it impacted the bed and finally formed a liquid marble [19,30]. The penetration time also increased with increasing APAP amount.

Figure 4.3 High speed video image sequences of single drop granulation on Coarse-MCC/Coarse-APAP mixtures: a) 10 % APAP, b) 90 % APAP.
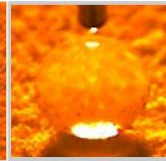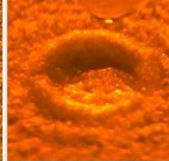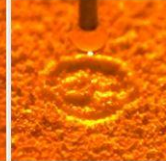
Coarse-MCC/Coarse-APAP	10 % (APAP)	30 %	70 %	90 %
Initial impact				
Final penetration				
Crater diameter increase (%)	36.1±8.3	36.7±8.9	35.8±5.4	38.1±6.3
Penetration time (ms)	67	155	300	910

Figure 4.4 The crater diameter increases and penetration times of each batch from Coarse-MCC/Coarse-APAP mixtures.

4.2.3. Fine-MCC/Fine-APAP mixtures

for the mixtures of Fine-MCC/Fine-APAP, the single drop granulation mechanism (see Fig. 4.5) turned out to be Tunneling for all proportions, which further substantiates our hypothesis about the significant effect of bed particle size on formation mechanism. Also, the penetration time for the droplet to completely penetrate through the powder bed increased, compared to the same proportions in the Coarse-MCC/Coarse-APAP mixtures. From the comparison of the crater diameter increase between the initial droplet and the finally formed crater (see Fig. 4.6), there is little change in the diameter (ranging from 6.6 % to 18.5 %). The crater diameter increase decreases with increasing APAP amount. With these mixtures, the droplet directly penetrated into the powder bed without spreading horizontally.

47
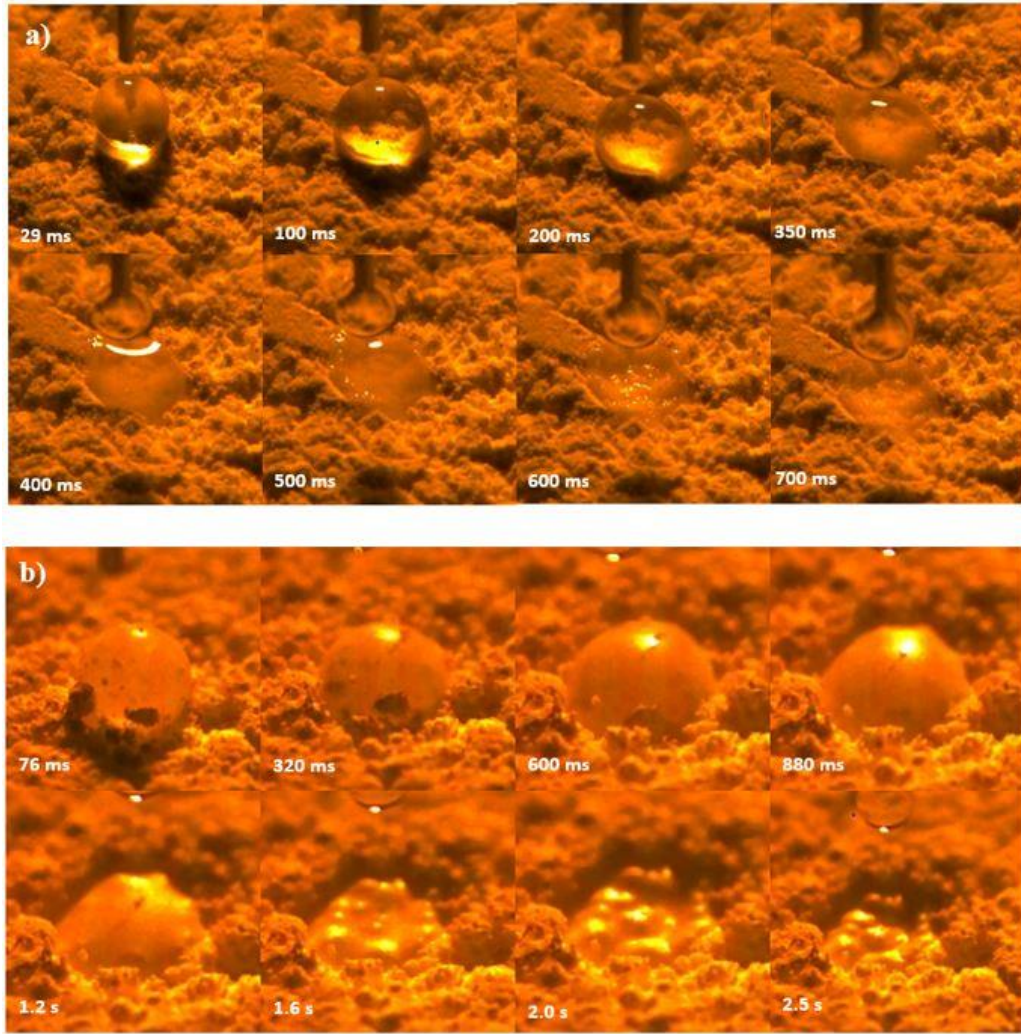
Figure 4.5 High speed video image sequence of single drop granulation on the Fine-MCC/Fine-APAP mixtures: a) 10 % APAP, b) 90 % APAP.
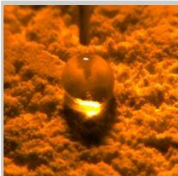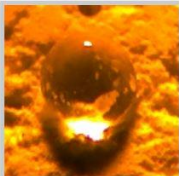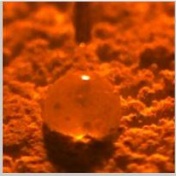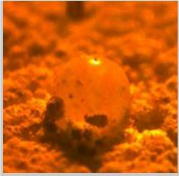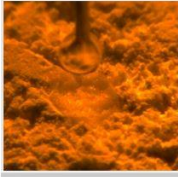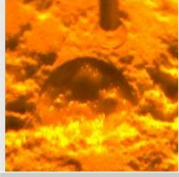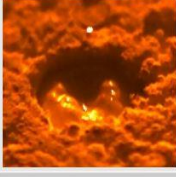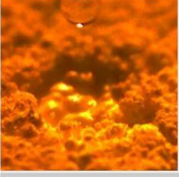
Fine-MCC/Fine-APAP	10 % (APAP)	30 %	70 %	90 %
Initial impact				
Final penetration				
Crater diameter increase (%)	18.5±6.3	13.4±5.6	7.4±5.0	6.6±4.9
Penetration time (ms)	671	1050	2300	2424

Figure 4.6 The crater diameter increases and penetration times of each batch from Fine-MCC/Fine-APAP mixtures.

4.2.4. Fine-MCC/Coarse-APAP mixtures

for granulation on mixtures of Fine-MCC/Coarse-APAP, the granulation sequences from proportions of 10 % and 90 % APAP are shown in Fig. 4.7. It is apparent that there is a difference in formation mechanisms between the two mixtures, with Tunneling occurring in 10 % APAP and Spreading occurring in 90 % APAP. By comparing the crater diameter changes in each proportion (see Fig. 4.8), a reverse trend of formation mechanisms was observed compared with mixtures of Coarse-MCC/Fine-APAP, as expected. Here, with the increase of APAP, the mechanism transitioned from Tunneling to Spreading, with the increase of the crater diameter increase from 14.9 % to 38.8 %.
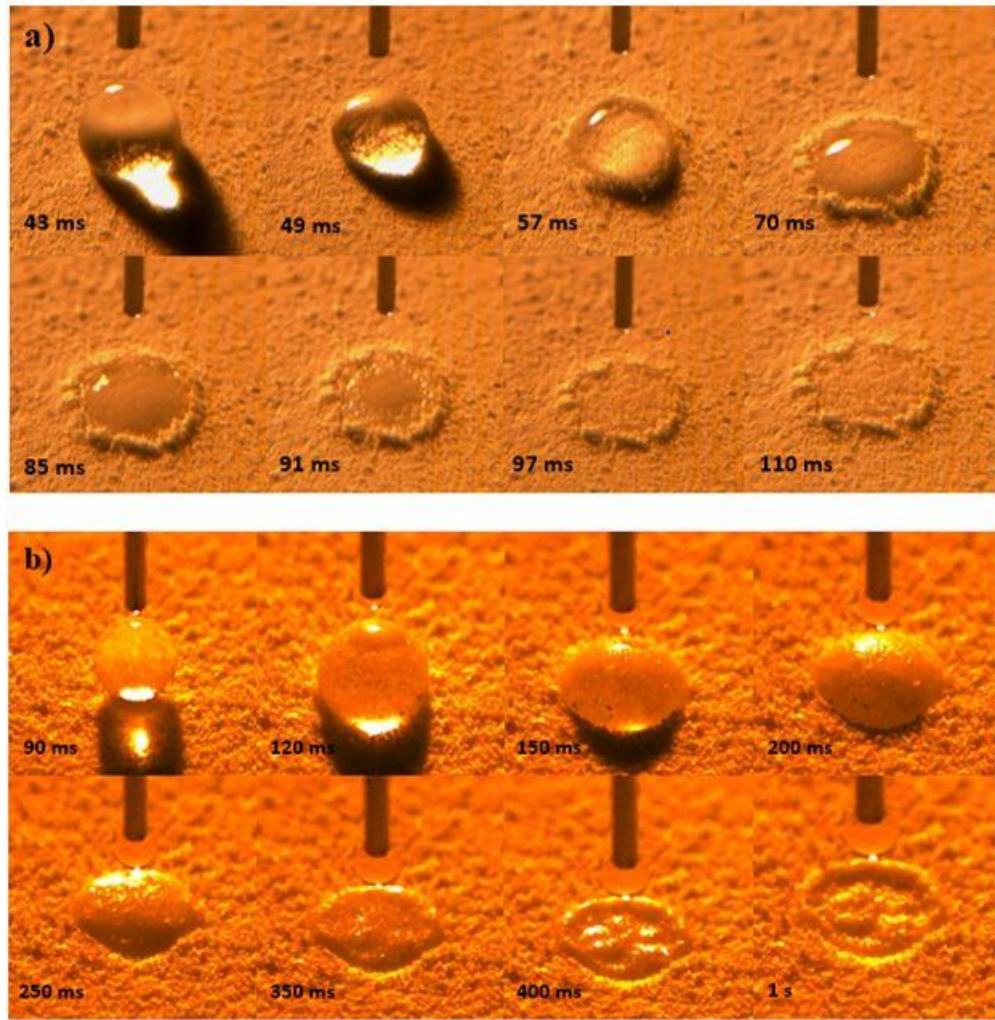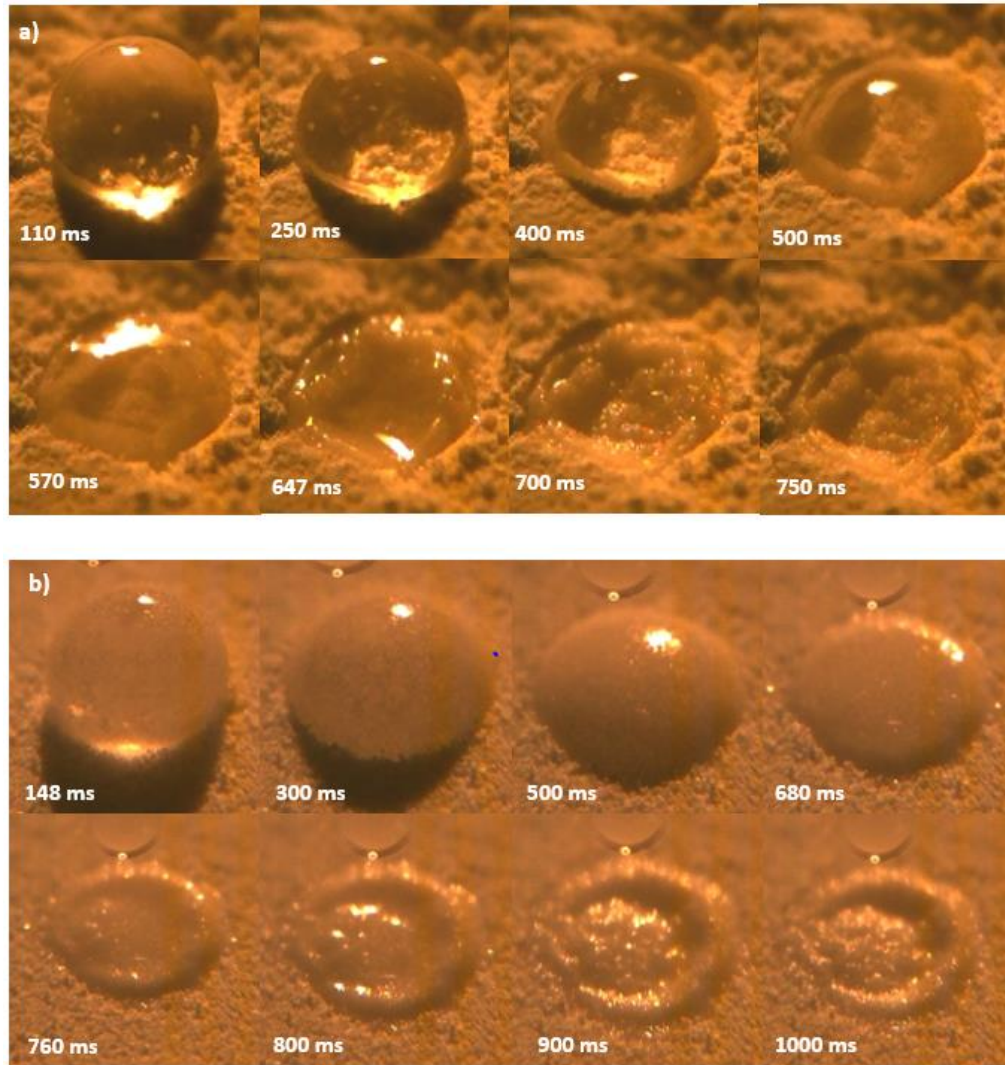
Figure 4.7 High speed video image sequence of single drop granulation on the Fine-MCC/Coarse-APAP mixtures: a) 10 % APAP, b) 90 % APAP.
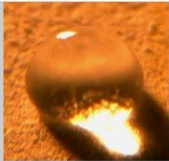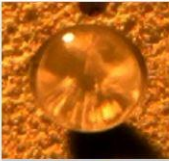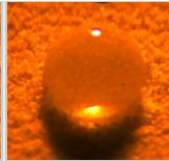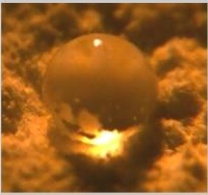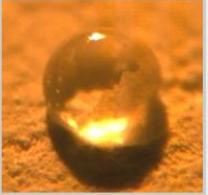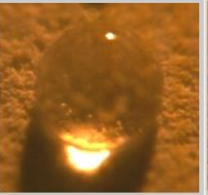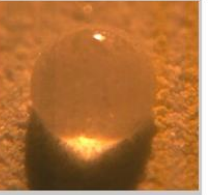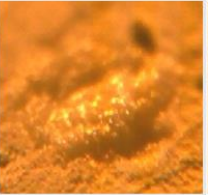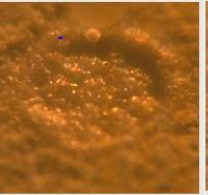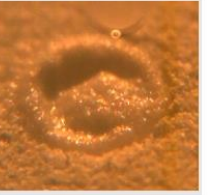
Fine-MCC/Coarse-APAP	10 % (APAP)	30 %	70 %	90 %
Initial impact				
Final penetration				
Crater diameter increase (%)	14.9 ± 6.8	15.0 ± 6.0	39.7 ± 8.7	38.8 ± 6.9
Penetration time (ms)	421	429	675	2404

Figure 4.8 The crater diameter increases and penetration times of each batch from Fine-MCC/Coarse-APAP mixtures.

4.3. Granule Morphology

The size and morphology of the granules from each batch of the granulation on Coarse-MCC/Fine-APAP mixtures is provided in Fig. 4.9. From the morphology of the granules, we can find that: 1) with the increase of APAP proportion, the granules from the batches generally become smaller in size, and 2) with the increase of APAP, the V.A.R of the granules generally decrease and become closer to 1, which means that the sphericity of the granules increase.

Batch (MCC/APAP)	100/0	90/10	80/20	75/25	70/30	65/35	60/40
Granule							
Formation mechanisms	Spreading	Spreading	Spreading	Spreading/Tunneling	Spreading/Tunneling	Spreading/Tunneling	Spreading/Tunneling
Morphology parameters	Size (mm): da: 7.18±0.56 hmax: 2.35±0.26	da: 5.66±0.39 hmax: 2.48±0.32	da: 4.98±0.27 hmax: 2.80±0.22	da: 4.21±0.37 hmax: 1.91±0.22	da: 4.26±0.31 hmax: 2.91±0.17	da: 3.79±0.19 hmax: 2.02±0.32	da: 4.04±0.17 hmax: 2.67±0.17
	Shape: H.A.R: 1.14±0.05 V.A.R: 3.09±0.49	H.A.R: 1.21±0.08 V.A.R: 2.11±0.35	H.A.R: 1.13±0.04 V.A.R: 1.79±0.15	H.A.R: 1.26±0.17 V.A.R: 2.21±0.16	H.A.R: 1.22±0.06 V.A.R: 1.47±0.13	H.A.R: 1.23±0.10 V.A.R: 1.91±0.23	H.A.R: 1.14±0.08 V.A.R: 1.52±0.08
Batch (MCC/APAP)	50/50	40/60	30/70	20/80	10/90	0/100	
Granule							
Formation mechanisms	Tunneling	Tunneling	Tunneling	Tunneling	Tunneling	Tunneling	
Morphology parameters	Size (mm): da: 3.34±0.19 hmax: 2.47±0.27	da: 3.39±0.28 hmax: 2.50±0.35	da: 3.19±0.30 hmax: 2.61±0.29	da: 2.88±0.24 hmax: 2.01±0.28	da: 2.85±0.28 hmax: 2.09±0.31	da: 3.75±0.25 hmax: 2.76±0.35	
	Shape: H.A.R: 1.16±0.12 V.A.R: 1.37±0.19	H.A.R: 1.11±0.07 V.A.R: 1.37±0.15	H.A.R: 1.18±0.10 V.A.R: 1.23±0.02	H.A.R: 1.07±0.05 V.A.R: 1.46±0.23	H.A.R: 1.09±0.11 V.A.R: 1.38±0.17	H.A.R: 1.39±0.16 V.A.R: 1.37±0.13	

Figure 4.9 Granule morphology from Coarse-MCC/Fine-APAP mixtures.

There are some exceptions to these general trends. for granules from 100% APAP, the size is larger than all of the granules made from mixtures of 50-90% APAP, and the granule shape is more irregular compared with other Tunneling-formed granules. This is mainly due to its primary particle size. Here, the appearance of the powder bed surface is clustered instead of flat, which means that the particles are more cohesive to form the dry aggregates. During the impact from the droplets, large aggregates are likely to be granulated and form granules with irregular shapes, as the protrusions cannot fully immerse in the liquid.

for granules from 50-100% APAP, the sphericity is nearly the same. At lower APAP proportions (0% to 20%), in the Spreading regime, the granules tend to be plate-like and

their V.A.R ranges from 1.79 to 3.09, while when the APAP proportion increases, the granules become rounder and look like balls. The V.A.R. of granules from 25%-40% APAP, in the transitional regime, ranges from 1.47 to 2.21. for granules from 50-100% APAP, for pure Tunneling, the V.A.R. is between 1.23 and 1.46. This also matches the results that in Spreading, the granules are plate-like, while in Tunneling, the granules are round [21]. Although this sharp distinction in shape occurs for the two pure regimes, the V.A.R. in the transitional regime has some values characteristic of Spreading, and some characteristic of Tunneling.
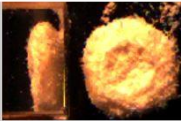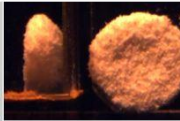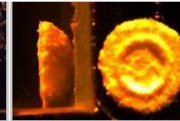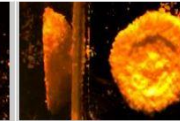
Coarse-MCC/Coarse-APAP	10 % (APAP)	30 %	70 %	90 %
Granules				
Formation mechanisms	Spreading	Spreading	Spreading	Spreading
Morphology parameters	Size (mm): d_a = 6.61±0.57 H_{max} = 2.32±0.28	d_a = 5.56±0.27 H_{max}= 2.44±0.23	d_a = 5.23±0.49 H_{max}= 2.21±0.29	d_a = 5.50±0.39 H_{max}= 2.21±0.22
	Shape: H.A.R.: 1.17±0.06 V.A.R.: 2.88±0.34	H.A.R.: 1.12±0.08 V.A.R.: 2.47±0.22	H.A.R.: 1.10±0.06 V.A.R.: 2.39±0.19	H.A.R.: 1.16±0.06 V.A.R.: 2.62±0.27

Figure 4.10 Granule morphology from Coarse-MCC/Coarse-APAP mixtures.

The size and morphology of the granules from Coarse-MCC/Coarse-APAP, Fine-MCC/Fine-APAP and Fine-MCC/Coarse-APAP are shown in Fig. 4.10, Fig. 4.11, and Fig. 4.12, respectively. The granules formed from beds of both coarse powders are all disk-shaped, with the V.A.R. ranging from 2.39 to 2.88, which is a typical Spreading indicator

53

(where Spreading occurs for V.A.R.'s greater than 1.5 to 2.2, and Tunneling occurs for lower values). Both the size and shape are similar with all batches, regardless of APAP amount.

on the other hand, the granules formed from beds made of both fine powders are much rounder. Here, with the increase of APAP amount, the sizes of the granules decrease slightly (from $d_a = 5.76$ mm to 3.96 mm). The V.A.R. values remain smaller, from 1.24 to 1.75 (with the increase of APAP proportion, V.A.R. values also decrease slightly from 1.75 to 1.24), which is a Tunneling indicator [21,63]. Moreover, the morphologies of some granules from fine/fine mixtures are more irregular, with protrusions around the surface, making them less smooth compared to granules from other mixture types.

The granules made from Fine-MCC/Coarse-APAP mixtures have a morphology trend that is inverse to that from Coarse-MCC/Fine-APAP mixtures, as expected. With the increase of APAP proportion, the overall particle size of the powder mixture increases. The granules turn from round balls into disk-like shapes, meaning the sphericity decreases (with V.A.R. values increasing from 1.83 to 2.07).

To summarize, the granule morphology was more affected by the overall particle size of the mixture rather than the mixture hydrophobicity. The granule morphology was also confirmed to be related to the formation mechanisms, as in previous work [21], where the

granules made from Spreading were plate-like, while those from Tunneling were more spherical in shape.
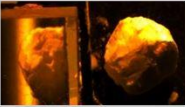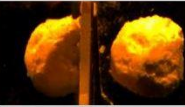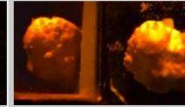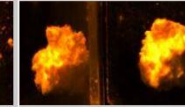
Fine-MCC/Fine-APAP	10 % (APAP)	30 %	70 %	90 %
Granules				
Formation mechanisms	Tunneling	Tunneling	Tunneling	Tunneling
Morphology parameters	Size (mm): d_a = 5.76±0.30 H_{max} = 3.30±0.21	d_a = 5.35±0.52 H_{max} = 3.54±0.29	d_a = 4.18±0.28 H_{max} = 3.36±0.41	d_a = 3.96±0.25 H_{max} = 3.23±0.34
	Shape: H.A.R.: 1.18±0.09 V.A.R.: 1.75±0.15	H.A.R.: 1.27±0.11 V.A.R.: 1.52±0.18	H.A.R.: 1.32±0.17 V.A.R.: 1.26±0.10	H.A.R.: 1.27±0.08 V.A.R.: 1.24±0.11

Figure 4.11 Granule morphology from Fine-MCC/Fine-APAP mixtures.
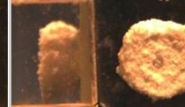
Fine-MCC/Coarse-APAP	10 % (APAP)	30 %	70 %	90 %
Granules				
Formation mechanisms	Tunneling	Tunneling	Spreading	Spreading
Morphology parameters	Size (mm): d_a = 5.77±0.44 H_{max} = 3.17±0.34	d_a = 5.75±0.33 H_{max} = 3.05±0.33	d_a = 6.09±0.46 H_{max} = 2.95±0.21	d_a = 5.38±0.43 H_{max} = 2.71±0.32
	Shape: H.A.R.: 1.19±0.05 V.A.R.: 1.83±0.23	H.A.R.: 1.17±0.11 V.A.R.: 1.93±0.19	H.A.R.: 1.17±0.09 V.A.R.: 2.07±0.17	H.A.R.: 1.18±0.04 V.A.R.: 1.99±0.15

Figure 4.12 Granule morphology from Fine-MCC/Coarse-APAP mixtures.

4.4.Relationship Between Penetration Time, formation Mechanism and Particle

Properties

Generally, with the increase of APAP proportion, the overall contact angle of the powder with water increases. Hapgood et al. [8] found that as the contact angle increases,

the penetration time increases, which is also consistent with our findings. and in their work, for the same contact angle of a certain mixture proportion, a trend of longer drop penetration time on formulations with a finer average particle size was also observed, which is also in agreement with our results.

By comparing the single drop granulation on all four different mixture types, we find that the primary factor that influences the formation mechanism is the overall particle size distribution of the mixture, where with the increase of the particle size, the formation mechanism transitioned from Tunneling to Spreading. on the other hand, this trend occurred regardless of the changing contact angle of the mixture. This means that the particle size is more dominant than the powder hydrophobicity in determining the granule formation mechanism in single drop granulation. The granule morphology is directly related to the formation mechanism, where the Spreading produced plate-like shapes with high V.A.R.'s, while Tunneling produced round shapes with low V.A.R.'s. The transitional mechanism (partially Spreading and partially Tunneling) produced hybrid granule shapes.

4.5. Conclusion

From this section, the penetration time, granule formation mechanisms, and granule morphology were studied for a powder mixture of microcrystalline cellulose (MCC) and acetaminophen (APAP). Both MCC and APAP have fine and coarse particle size,

respectively, while the water-powder contact angle of APAP is higher than that of MCC, meaning MCC is more hydrophilic than APAP.

In the Coarse-MCC/Fine-APAP mixtures, with the increase of proportion of APAP, both the first and second penetration time increase. When the proportion of APAP reaches 50%, since it is hard to recognize the second penetration time due to the Tunneling mechanism that occurs in a relatively finer powder bed, only the first penetration time can be recognized, and there is not a clear trend. for high proportions of MCC or APAP (100 % or 90 %), the penetration time is a little irregular, which is likely due to the improper mixing of the powder bed that can arise from the large difference in amounts between the two components. for the other three mixture types, with the increase of APAP proportion, the total penetration time increased as well. However, the drop penetration times are much longer in mixtures with fine components than in those with coarse components.

The formation mechanisms directly depend on the particle size distributions of the mixtures. In Coarse-MCC/Coarse-APAP mixtures, only Spreading occurred, while in Fine-APAP/Fine-APAP mixtures, only Tunneling occurred. for Coarse-MCC/Fine-APAP and Fine-MCC/Coarse-APAP mixtures, the formation mechanism transitioned from Spreading to Tunneling with the decrease in the overall particle size of the mixture.

The granule morphology was more affected by the particle size of the mixture rather than the mixture hydrophobicity, where the granules formed from coarser mixtures were plate-like, while the granules formed from finer mixtures were rounder.

CHAPTER 5. PRODUCT STRUCTURE FROM SINGLE DROP GRANULATION

5.1.Introduction

In this chapter, the granules made from Coarse-MCC/Fine-APAP mixtures will be characterized by SEM (scanning electronic microscope) for the surface structure and by micro-CT for the internal structure, respectively. Additionally, the bed surface will be scanned by micro-CT to investigate the packing structure of the powder bed for comparison with the granule internal structure. The results will show the effects of changing the component proportions in the mixtures on the internal structures of both the powder bed surface and the granules.

5.2.Granule Surface Structure

The surface microstructures of the granules made from 100% MCC, 70% MCC and 100% APAP are shown in Fig. 5.1. From the lower magnification of the SEM images, it can be seen that granules from 100 % MCC were formed loosely compared with granules from 100 % APAP, while the packing of granules from 70 % MCC were in between. From the higher magnification of the SEM images, the surface roughnesses are different for the MCC and APAP primary particles. The MCC particles have micro textures on their surface, making them rougher, while the APAP particles are relatively smoother. The primary particle sizes range from 5 to 50 μm for APAP and from 10 to 100 μm for MCC, which is

consistent with the particle size measurement results from measurement by the optical

microscope (Malvern Morphologi G3SE).
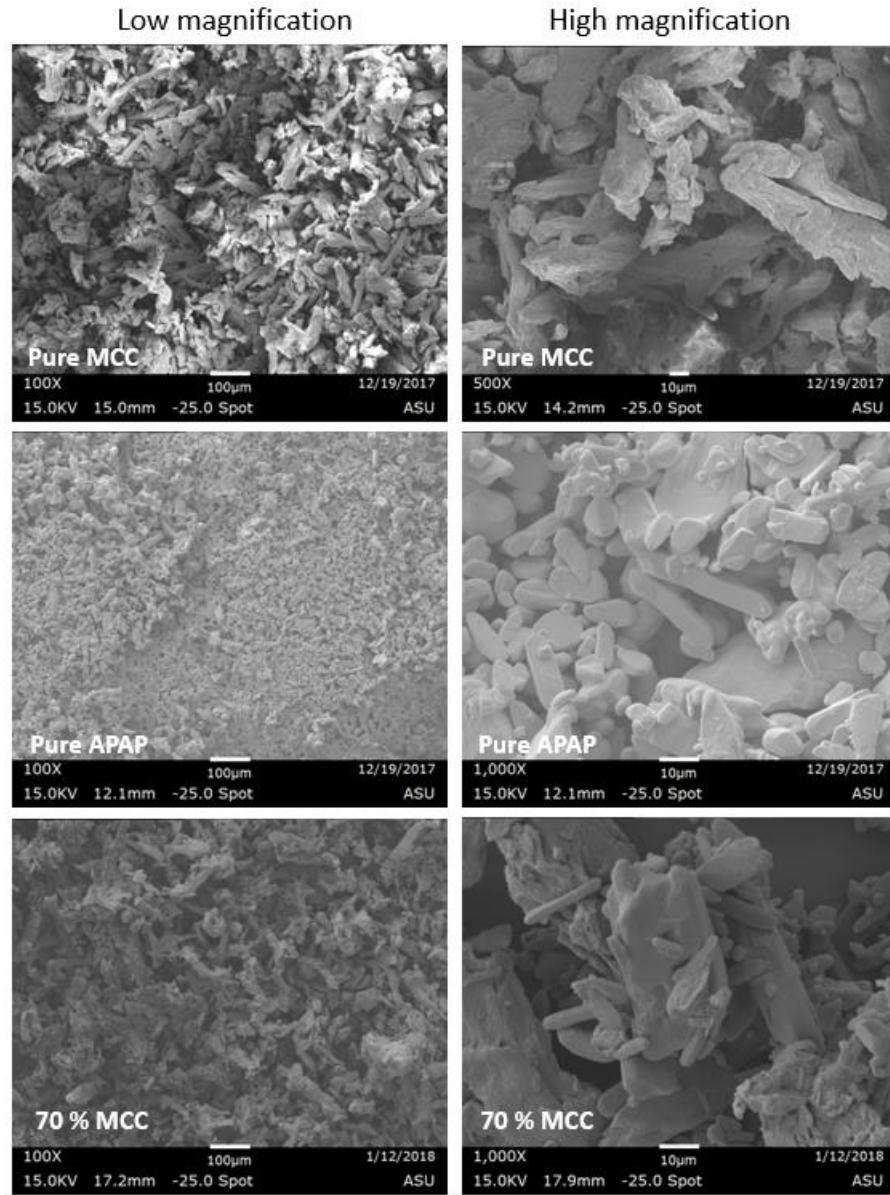
Figure 5.1 SEM images of a pure Coarse-MCC granule, pure Fine-APAP granule and 70 % MCC granule, from top to bottom, with low magnification (left), and high magnification (right).

5.3. Granule and Bed Packing Internal Structure

5.3.1. Granule Internal Structure

The porosities of each sub region from each sample were quantified. The porosities of pure MCC from the sub regions range from 67.5 % to 69.6 %, while the porosities of pure APAP from the sub regions range from 59.2 % to 62.0 %. The percentage difference of the porosities in pure MCC and APAP granules are only 3.1 % and 4.7 %, respectively. Thus, the choice of sub region does not have a significant influence on the total porosity with the pure component granules. However, for granules of 70 % MCC, the porosities vary slightly more, ranging from 56.8 % to 62.8 %, resulting in a percentage difference of 10.0 %. The overall porosities of each sample were calculated by averaging the porosities of all the sub regions, and are summarized in Table 5.1.

Sample	Pixel size (μm)	Average porosity (%)
Pure MCC 1	3.38	68.6 ± 0.8
Pure MCC 2	3.23	68.8 ± 0.2
Pure APAP 1	1.96	61.5 ± 0.4
Pure APAP 2	2.23	60.5 ± 0.9
70 % MCC 1	2.32	59.9 ± 1.6
70 % MCC 2	1.89	61.8 ± 1.4
90 % MCC	2.77	68.2 ± 0.6

Table 5-1 The average porosity of each granule sample, with standard deviation.

The porosities of each sub volume from pure MCC are very consistent. From the representative slice (see Fig. 5.2a), the internal structure is loose and the pores are uniformly distributed among the matrix. There are diffuse pore networks connected with

each other. However, there are some local looser pore areas appearing in some slices (see Fig. 5.2b), which are minimal compared with the whole granule internal structure. The overall porosity of MCC granules, obtained by averaging the two samples, is 68.7 % ± 0.6 %.
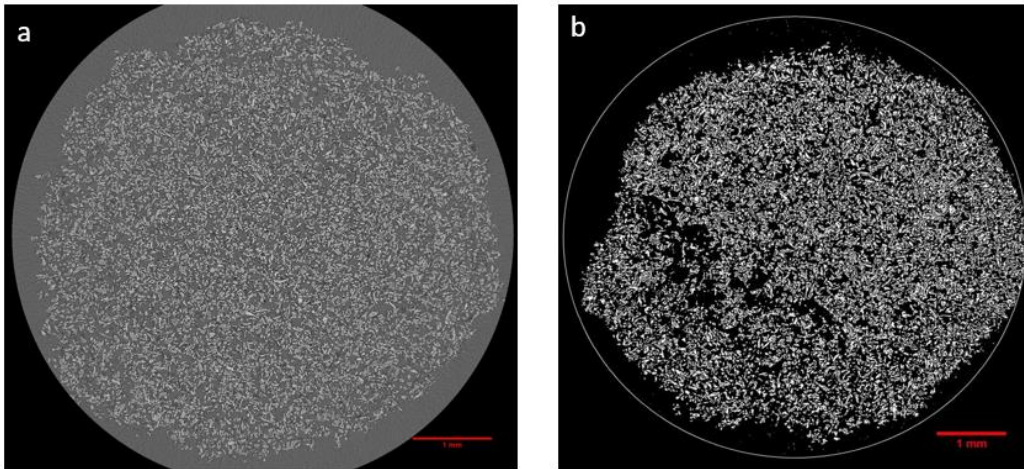
Figure 5.2 Grayscale images of the representative internal structure of a pure Coarse-MCC granule (with overall porosity of 68.7 % ± 0.6 %): a) slice with uniform structure, b) slice with large pores.

From the representative slices of pure APAP granules, the internal structure is denser compared with that of pure MCC granules. The packing of the particles is more compact. However, there are a number of large, discrete voids surrounded by a dense matrix (see Fig. 5.3a). This finding is consistent with results from single drop granulation on ultra-fine particles from Davis et al. [37]. The sub regions without the large voids have an average porosity of 60.8 % ± 0.4 %, while the average porosity of the regions with the voids increases slightly to 61.8 % ± 0.3 %.

The granules made from heterogeneous mixtures were more complex. The internal structure of a granule made from 70 % MCC is shown in Fig. 5.4. Here, there are a few local dense regions appearing inside the granule. Among these regions, one that contains the entire dense area has a porosity of 56.8% (see Fig. 5.4a), compared to that of the rest of the areas with a higher average porosity of 61.6 % ± 0.9 %. However, a region with a mix of dense and loose portions (see Fig. 5.4b) has a porosity of 58.8 %, which is in between the porosities of the completely dense area and that of the normal areas. To further investigate the relationship between the amount of MCC and the internal structure, a granule made from 90 % MCC was also scanned, and a representative slice of its internal structure is shown in Fig. 5.5. Here, it can be seen that the internal structure of the 90 % MCC granule is very close to that of the pure MCC granules. The overall porosity of the 90 % MCC granule is 68.2 % ± 0.6 %, compared to that of the pure MCC granule, which is 68.7 % ± 0.6 %.

We expect the porosity difference between the two kinds of granules to be attributed to the large difference in primary particle size and subsequent influence on the formation mechanism. Based on the granulation formation mechanisms mentioned in Chapter 4, the powder bed of pure Coarse-MCC is composed of individually packed particles and less cohesive, resulting in flat Spreading-formed granules. Granules made from pure Fine-APAP were formed through the Tunneling mechanism due to the fine particle size and its higher contact angle. Fine particles are more cohesive than larger and coarser particles,

which can create strong cohesive forces and make the powder bed more complex. This leads to different density regions throughout the structure and their interactions with the liquid will also differ. During Tunneling, as occurs with APAP, the droplet's penetration into the loose, fine and cohesive bed is driven by capillary force. Dry aggregates on the bed surface were sucked into the droplet due to the stronger capillary force compared with the adhesive force between those aggregates, and they then migrated inside the droplet. This is a similar phenomenon observed by Emady et al. [21], where the particles and aggregates picked up from the bottom surface re-accumulate inside the droplet, which may explain the formation of randomly distributed large voids.

The bed preparation also contributes to the voids formation in pure Fine-APAP granules. The APAP powder was sieved through a 2 mm sieve, with the purpose to achieve a relatively uniform distribution of particle clusters. However, due to its fine and highly cohesive nature, during the bed preparation of pure APAP, the widely distributed aggregates may still form a relatively inhomogeneous powder bed. Thus, the powder bed may already consist of macro-voids before the drop granulation.

for heterogeneous mixture powder beds, with increasing the amount of APAP into the mixture to 10 %, the overall porosity only decreased by 0.7 %, while with increasing the amount of APAP to 30 %, the overall porosity decreased by about 10.4 %, which is almost down to the porosity of pure APAP. The overall porosities of all granules from different

proportions are illustrated in Fig. 5.6. The general trend is that the porosity decreases with increasing APAP percentage. However, the overall porosity of granules from 70% MCC that includes all measured regions in the granules (shown by column "70% MCC (2)") is slightly smaller than that from pure APAP granules. This is due to the existence of those dense regions in the 70% MCC granules. To better interpret the effects of the APAP proportion on the granule internal structure, we choose to exclude those dense regions, since the volume of those re- gions are very small compared with the total volume (only less than 20%). Additionally, the porosity of the dense regions (56.8%) is even smaller than that of pure APAP (60.8%), which hints at a more com- plicated aggregation effect that has not been investigated. The spaces created by larger MCC particles may be filled by the smaller APAP particles, resulting in an even denser packing condition than pure APAP granules, which should be considered in future work as a study of more efficient packing.

There also appears to be a significant transition in the porosity from granules made of 90 % MCC to 70 % MCC. This may be due to the transition of formation mechanism from Spreading to Tunneling, which occurs between the proportion (MCC/APAP) of 75/25 to 60/40. Granulation that occurred in the mixture containing 90 % MCC is still Spreading, so both the internal structure appearance and the measured porosity are much closer to those of pure MCC. However, for 70 % MCC samples, although the amount of APAP is only 30 %, Tunneling is already starting to occur in this proportion. The formation of the granule becomes more complex, leading to the inhomogeneity of the internal structure, due

65

to the unpredicted interaction between the two kinds of particles during Tunneling combined with Spreading.
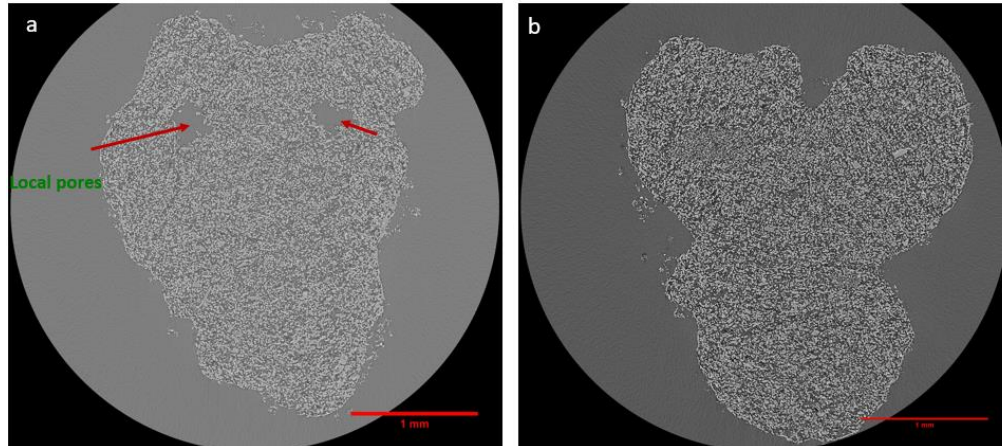
Figure 5.3 Grayscale images of the representative internal structure of a pure Fine-APAP granule: a) slice with large local pores (with porosity of 61.8 % ± 0.3 %), b) slice with uniform structure (with porosity of 60.8 % ± 0.4 %).
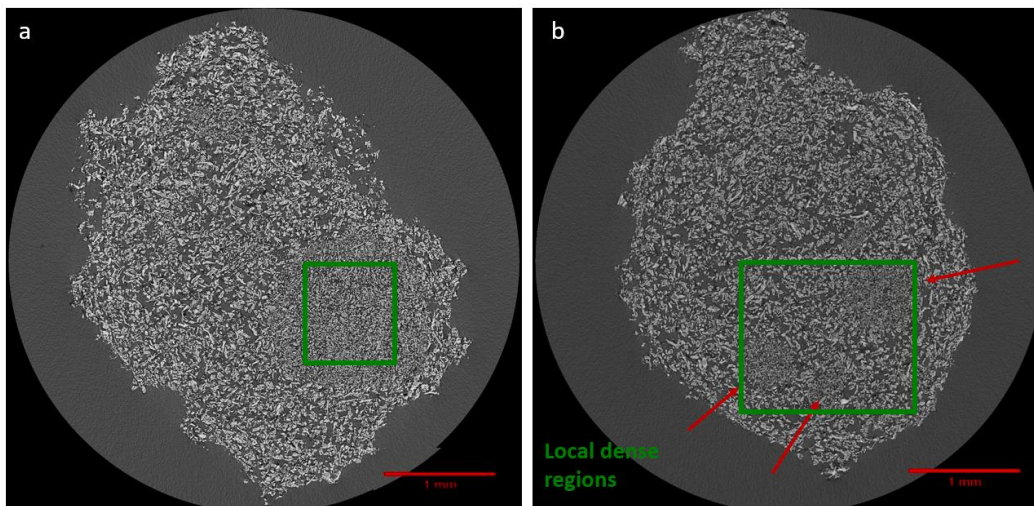
Figure 5.4 Grayscale images of the representative internal structure of a 70 % Coarse-MCC (30 % Fine-APAP) granule: a) slice with a big dense region (indicated by the green rectangle, with porosity of 56.8%), and b) slice with multiple small dense regions (indicated by the green rectangle, with porosity of 58.8%). The overall porosity of the rest of the non-dense regions is 61.6 % ± 0.9 %.
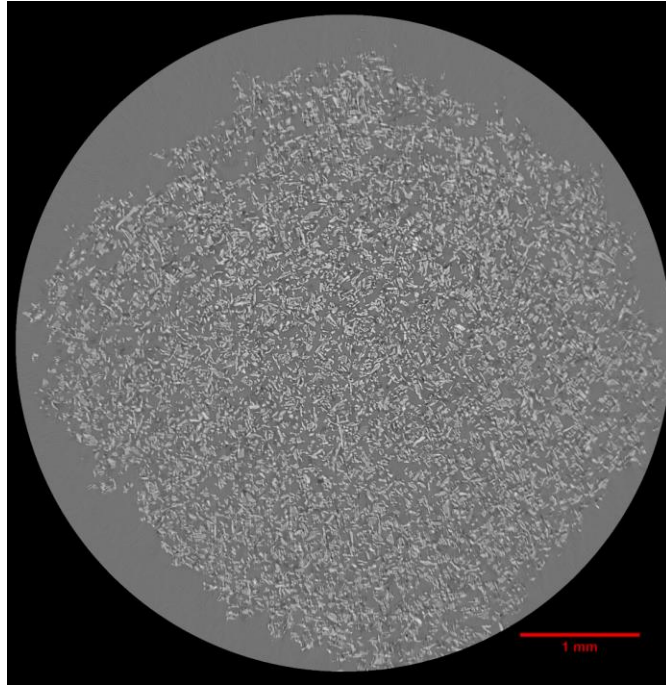
Figure 5.5 Grayscale image of the representative internal structure of a 90 % Coarse-MCC (10 % Fine-APAP) granule (with porosity of 68.2 % ± 0.6 %).
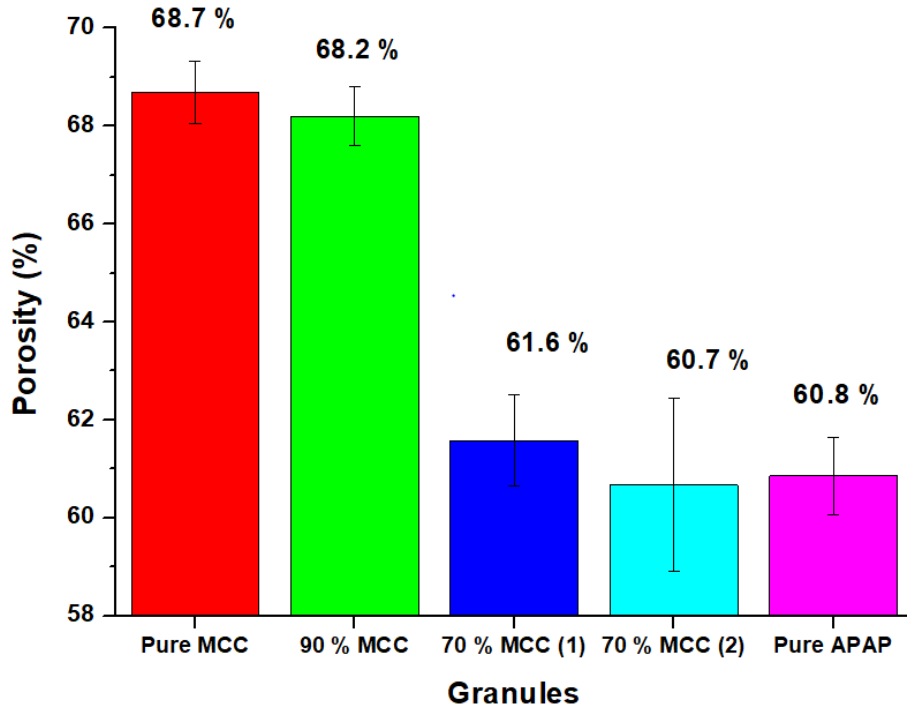
Figure 5.6 Summary of the overall porosities of granules from different proportions. Since 70% MCC includes dense regions, two different average porosities are calculated: 70% MCC (1) excludes the dense regions, while 70% MCC (2) includes all measured regions.

The localized clustering and presence of large voids can be visualized by 3D volume rendered images of the internal structure of granules (see Fig. 5.7). By comparing the 3D images in Fig. 5.7, it can be seen that the pores in the MCC granule are larger and more homogeneous (see Fig. 5.7a), while the pores in the APAP granule are smaller, with the existence of some macro-voids (see Fig. 5.7c), and the mixture granule of 70% MCC (see Fig. 5.7b) has an intermediate structure with characteristics of both pure substances. This means that granules made from pure MCC are looser than granules made from pure APAP.
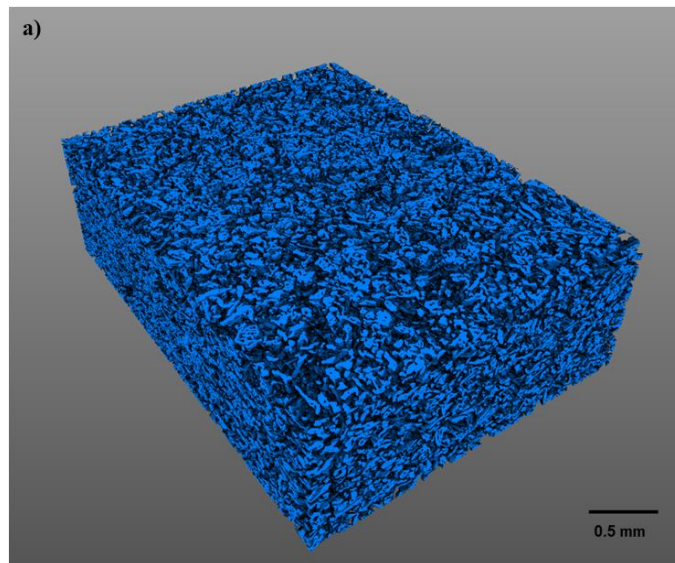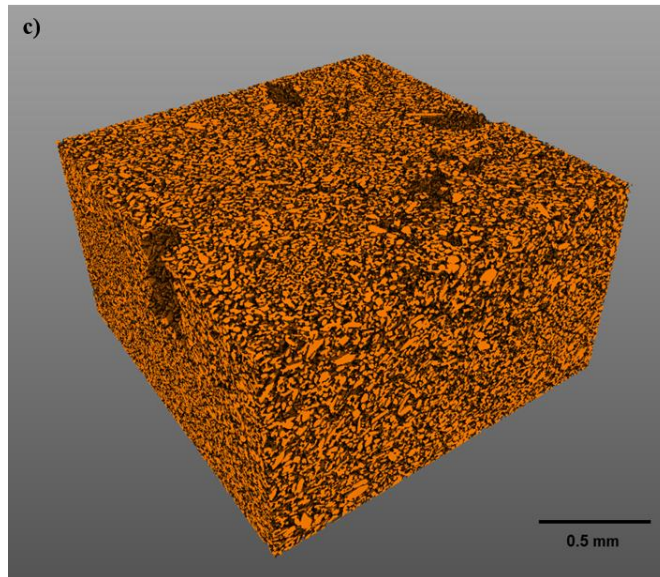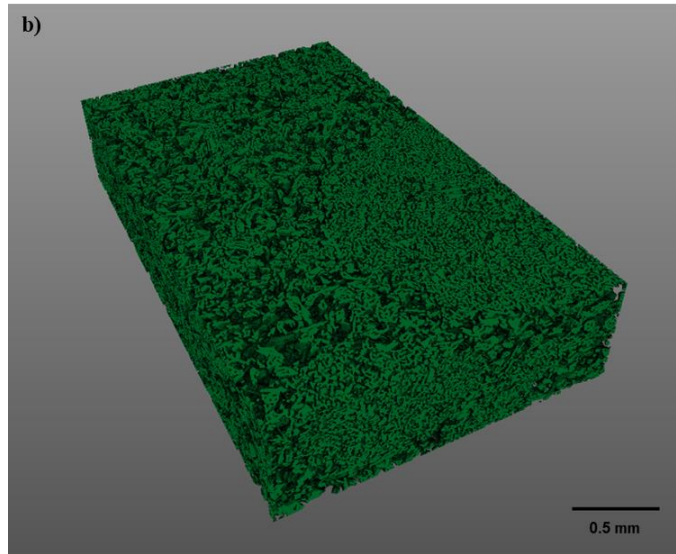
Figure 5.7 3D Volume renderings of a) pure Coarse-MCC, b) 70% MCC, and c) pure Fine-APAP granule showing the change in pore network and structure.

To summarize the information in the figures and tables, there is a large difference in internal structure between MCC and APAP. The overall porosity of MCC is larger than that of APAP, while the porosities of the heterogeneous mixtures are in between. There is

a significant drop in the overall porosity when moving from the Spreading to the Tunneling mechanism. We hypothesize that the big transition point of the porosity should be in between 90 % MCC and 70 % MCC, and close to 75 % MCC, where the transition from Spreading to Tunneling starts. Thus, the porosities of granules made from 70 % to 0 % MCC should be very close, consistent with the pure Tunneling mechanism. The bed packing structure, along with particle size, explain the formation mechanism and corresponding granule shape. Now we can add to this information the difference in granule internal structure and porosity. We conclude that the internal structure of the granules is mainly determined by the formation mechanism, which is strongly influenced by the structure of the powder bed and the particle size.

5.3.2. Bed Packing Structure

The internal porosities of two powder bed packing columns taken from different areas in a single Coarse-MCC/Fine-APAP mixture of 30 % APAP proportion are shown in Table 5-2. The porosities of two different regions within each sample is consistent (~81.1 % for one sample and ~83.2 % for a second sample), and fairly consistent at ~81-83 % within the same powder bed. By comparing the porosities of the granules made from the same proportion of APAP [63] which are only around 60 %, the wet granulation densifies the

70

internal structure during the formation of granules by decreasing the porosity by around

20 %.

Material	Dimensions	Total Volume (μm^3)	Porosity (%)
30 % APAP dry powder bed - sample 1	900x1600x900	3.08E+10	81.08
	1375x1150x1100	4.13E+10	81.06
30 % APAP dry powder bed - sample 2	900x1600x900	3.08E+10	83.24
	1100x1150x1100	3.30E+10	83.25

Table 5-2 The internal porosity of the powder bed packing for 30 % APAP in a Coarse-MCC/Fine-APAP mixture.

The micro-CT results, with a 2D cross-section of granules made from 30 % APAP, 2D cross-section of the powder column made from 30 % APAP, and a 3D reconstruction of the whole powder column, are shown in Fig. 5.9 a, b and c, respectively. As revealed by the internal structure of the powder bed, there are dense regions existing in the mixture (indicated by blue arrows in Fig. 5.9b). Dense regions of difference sizes are randomly distributed in the mixture (see Fig. 5.9c). Most of the dense regions are located in the upper half of the column, where the granules are typically formed when the droplet impacts the surface of the powder bed. There are also several denser regions observed in granules made from the same proportion in the study on granules [63] (shown in Fig. 5.9a). This indicates that during the preparation of the powder mixture, an inhomogeneous powder packing is already created before the wet granulation. Thus, the dense regions in the granules are likely generated directly from the same regions in the dry powder bed.

In this study, the internal structure of the powder bed was only characterized for one mixture from one mixture type (Coarse-MCC/Fine-APAP), and the granules formed directly from this powder bed were not characterized. for a more complete understanding of how the powder packing influences the formation mechanism and subsequently formed granule, powder bed internal structure from both coarse mixtures (exhibiting Spreading) and fine mixtures (exhibiting Tunneling) should be investigated. Also, the internal structures of the granules should be analyzed from the same powder bed to directly compare the powder bed packing and granule porosity.
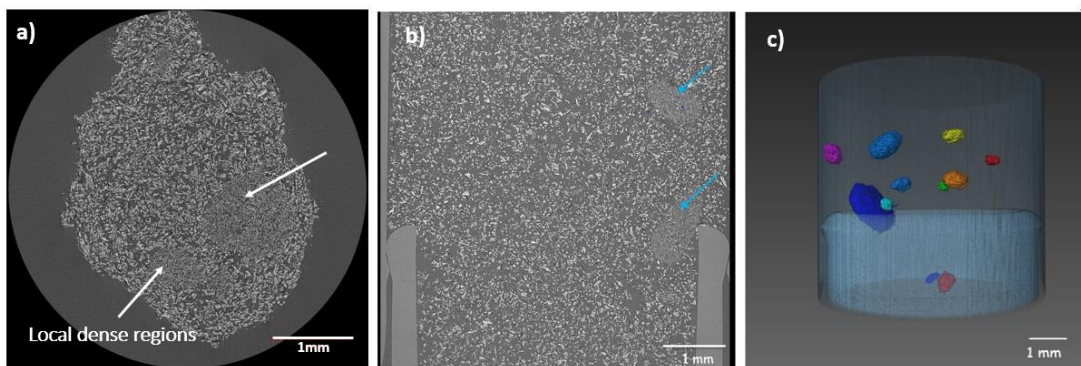
Figure 5.8 a) 2D cross-section of a granule, b) 2D cross-section of the powder packing, and c) 3D reconstruction of the whole powder packing column (with dense regions highlighted in different colours).

5.4. Conclusions

According to SEM images of granules from Coarse-MCC/Fine-APAP mixtures, the MCC and APAP powders have different surface roughnesses, showing different packing for different granules, which is consistent with the internal structure results.

The internal structures of granules made from pure MCC, pure APAP, and heterogeneous mixtures from Coarse-MCC/Fine-APAP mixtures, as characterized by micro-CT, show that pure MCC has an evenly distributed pore network, while pure APAP has many smaller pores but also several large isolated voids. The porosity of the granules produced from the Spreading mechanism is larger than that of the granules produced from the Tunneling mechanism. With the increase of the amount of APAP, the granules made from heterogeneous mixtures become more complex, especially for those in the transitional mechanisms that exhibit characteristics of both Spreading and Tunneling. Here, the internal structure is relatively non-uniform, containing both dense and loose regions.

for internal structure of the powder bed surface from the Coarse-MCC/Fine-APAP mixture, the internal structure of the powder packing at 30% APAP appears to have several dense regions within the mixture, which are also found in the granules made from the same APAP proportion. It is assumed that those dense regions already existed during the bed preparation stage, even before the wet granulation. Additionally, the overall porosity of the powder bed is approximately 20% lower than that of the granules made from the same mixture. This indicates that the wet granulation densified the internal structure from the bed surface to the granules formed.

CHAPTER 6. PRODUCT CONTENT UNIFORMITY FROM SINGLE DROP

GRANULATION

6.1.Introduction

In this chapter, the content uniformity of the MCC-APAP system will be investigated through UV-vis spectrometry. Both the uniformity of the powder bed surface and the granules formed will be examined to see if there is improper mixing during the bed preparation or preferential wetting of one component, respectively. The results will reveal the relation between the content uniformity and different proportions of MCC/APAP, which will be useful in the design and prediction of granulation of heterogeneous powder materials.

6.2.Results

The content uniformity of APAP from the powder bed surface is compared with the content uniformity of APAP in the granules from the same ingredient proportion to investigate the potential origin of the content uniformity discrepancies. The results from four different mixture types are discussed individually and compared to each other to determine the causes of granule inhomogeneity.

for Coarse-MCC/Fine-APAP, mixtures were tested in 10 % increments as a benchmark to determine the content uniformity trend. The comparison between the experimental and theoretical results are demonstrated in Fig. 6.1, where both the granule and bed surface

uniformities with their standard deviations are shown. for the overall trend, it appears that

with the increase of the APAP amount above 60 %, both the content uniformities of the

granules and the bed surface are compromised. The numerical values are provided in Table

6-1. The average deviation, *V*, of the actual content compared with the theoretical value is

calculated as:

$$\mathbf{V} = \sqrt{\frac{\sum_{i}^{n} (x_i - \hat{x})^2}{n - 1}} \tag{12}$$

where x_i is the actual measurement and $\hat{x}$ is the theoretical value of APAP in each

mixture. Specifically, the average deviation between the real APAP amount on the powder

bed surface and in the granules becomes larger as the APAP amount increases (8.6 %, 12.5

% and 16.4 % for 70 %, 80 % and 90 % APAP in the bed surface; 14.1 %, 36.3 % and 25.1

% for 70 %, 80 % and 90 % APAP in the granules). Additionally, the standard error of

each measurement also increases when the APAP amount is above 50 %, indicating a

potential heterogeneous behaviour of the powder mixing and granulation in higher APAP

proportions.
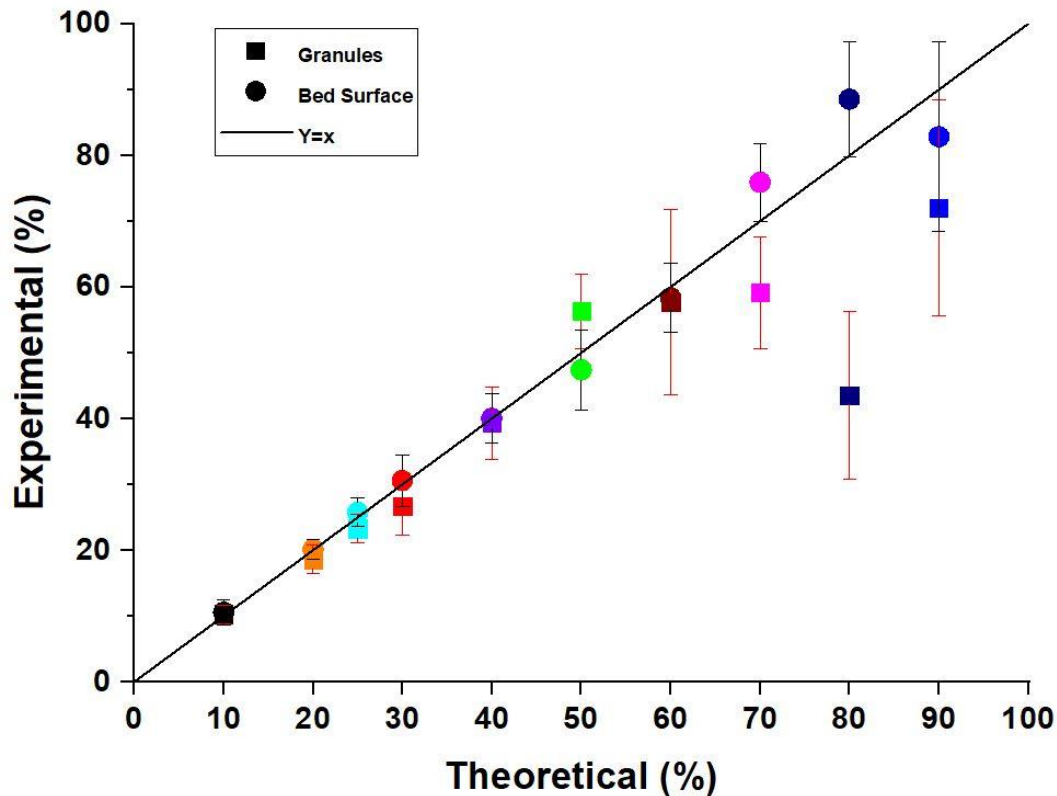
Figure 6.1 Composition of granules and powder bed surface containing different proportions of APAP with MCC from Coarse-MCC/Fine-APAP mixtures.

By normalizing the API (APAP) content in the granule by that in the bed surface (demonstrated in Table 6-1), there is a noticeable difference between the content uniformity of the granules and the bed surface when the APAP proportion increases above 60 %. The actual APAP amounts in the granules are all lower than in the bed surfaces. Thus, the granules incorporate less APAP than MCC during their formation. This indicates that preferential wetting of the more hydrophilic component (MCC) occurs in single drop

granulation of binary mixtures with components of varying hydrophobicity, at least in the

coarse/fine mixture type.

Coarse-MCC/ Fine-APAP	10 % (APAP)	20 %	25 %	30 %	40 %
Theoretical (% APAP)	10	20	25	30	40
Bed surface (% APAP)	10.6 ± 1.9	18.4 ± 2.7	25.7 ± 2.2	30.6 ± 3.9	40.0 ± 3.8
Average deviation in bed surface vs. theoretical (%)	1.9	1.6	2.3	3.9	5.4
Granules (% APAP)	10.3 ± 1.4	18.6 ± 2.2	23.3 ± 2.1	26.7 ± 4.4	39.3 ± 5.5
Average deviation in granules vs. theoretical (%)	1.5	2.6	2.7	4.8	5.4
Normalized API	0.97 ± 0.22	1.01 ± 0.19	0.91 ± 0.11	0.87 ± 0.18	0.98 ± 0.17
Coarse-MCC/Fine-APAP	50 % (APAP)	60 %	70 %	80 %	90 %
Theoretical (% APAP)	50	60	70	80	90

Bed surface (% APAP)	47.4 ± 6.0	58.3 ± 14	75.9 ± 6.0	88.5 ± 8.7	82.8 ± 14.4
Average deviation in bed surface vs. theoretical (%)	6.6	5.5	8.6	12.5	16.4
Granules (% APAP)	56.3 ± 5.7	57.7 ± 14	59.1 ± 16.5	43.5 ± 22.0	72.0 ± 16.5
Average deviation in granules vs. theoretical (%)	8.8	12.9	14.1	36.3	25.1
Normalized API	1.19 ± 0.19	0.99 ± 0.34	0.78 ± 0.23	0.49 ± 0.25	0.87 ± 0.25

Table 6-1 Measured APAP weight percentage for each proportion in powder bed surface and granules from Coarse-MCC/Fine-APAP mixtures (averages with standard deviations for three replicates for each mixture).

for Coarse-MCC/Coarse-APAP, Fine-MCC/Fine-APAP and Fine-MCC/Coarse-APAP mixtures, five proportions are selected: 10 %, 30 %, 50 %, 70 % and 90 % APAP.

In Coarse-MCC/Coarse-APAP mixtures, for lower APAP amounts (10 % and 30 %), the APAP contents in both the bed surface and the granules from experiments are very close to the theoretical values (see Fig. 6.2). When the APAP amount increases to 70 % and 90 %, there is a slight compromise in the content uniformities of the granules, which are also sub-potent (lower than the theoretical values). The numerical values are provided

in Table 6-2. Compared to the results from Coarse-MCC/Fine-APAP mixtures, even though content uniformity is compromised in both cases, the compromised level in Coarse-MCC/Coarse-APAP is less significant for higher APAP proportions. for lower APAP proportions, the APAP compositions for both mixture types are close to the theoretical values. The average deviation vs. the theoretical values in Table 6-2 are all lower than those from Coarse-MCC/Fine-APAP mixtures. for lower APAP amounts (10 % and 30 %), since APAP only occupies a small portion of the whole mixture, changing from fine APAP to coarse did not greatly affect the overall particle size of the bed, so the effect of particle size on content uniformity is small. However, for higher APAP amounts, changing from fine APAP to coarse increases the overall particle size of the powder bed due to the higher APAP occupancy in the whole mixture (70 % and 90 %). Also, within the higher APAP ranges, larger discrepancies in the content uniformity occur. An initial hypothesis was made based on the comparison between Coarse-MCC/Coarse-APAP and Coarse-MCC/Fine-APAP mixtures: increasing the mixture bed particle size will result in a more uniform ingredient content.
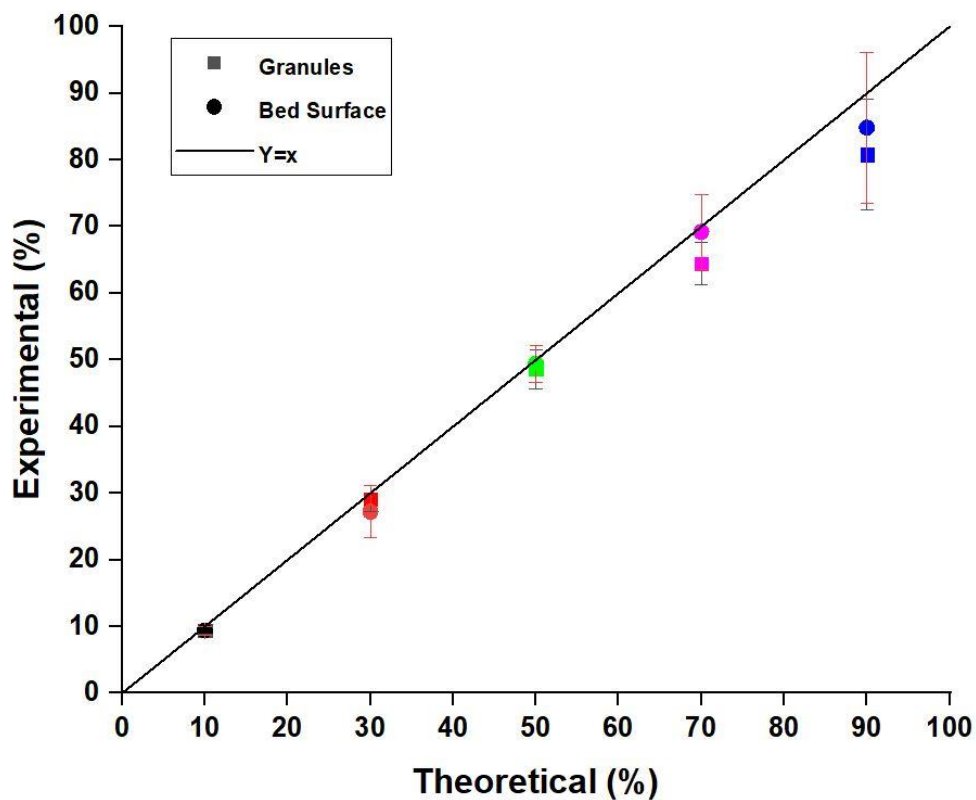
Figure 6.2 Composition of granules and powder bed surface containing different proportions of APAP with MCC from Coarse-MCC/Coarse-APAP mixtures.

Coarse-MCC/ Coarse-APAP	10 % (APAP)	30 %	50 %	70 %	90 %
Theoretical (% APAP)	10	30	50	70	90
Bed surface (% APAP)	9.4 ± 0.7	27.2 ± 3.9	49.4 ± 2.8	69.2 ± 5.6	84.8 ± 11.3
Average deviation in bed surface vs. theoretical (%)	0.9	3.6	2.9	5.7	6.62

Granules (% APAP)	9.5 ± 0.6	29.1 ± 2.0	48.6 ± 3.0	64.4 ± 3.2	80.8 ± 8.2
Average deviation in granules vs. theoretical (%)	0.8	2.2	3.3	6.8	8.9
Normalized API	1.01 ± 0.09	1.07 ± 0.17	0.98 ± 0.08	0.93 ± 0.09	0.95 ± 0.16

Table 6-2 Measured APAP weight percentage for each proportion in powder bed surface and granules from Coarse-MCC/Coarse-APAP mixtures (averages with standard deviations for two replicates for each mixture).

In Fine-MCC/Fine-APAP mixtures, for the lowest APAP amount (10 %), the content uniformities of both the bed surface and the granules from experiments are close to the theoretical values (see Fig. 6.3). With the increase of APAP amount, the content discrepancies compared with the same APAP proportion in the other two mixture types (coarse/fine and coarse/coarse) increase, especially for the proportions of 30/70 and 10/90. Similar to the mixtures of Coarse-MCC/Fine-APAP, a non-uniform distribution of the binary components also exists in the powder bed before granulation, causing heterogenous mixing of the APAP with the MCC during granule formation. However, the preferential wetting effect was almost negligible for coarse/coarse and fine/fine mixtures, as demonstrated by the normalized API percentages that are close to 1 (see Table 6-2 and Table 6-3).

for Fine-MCC/Fine-APAP mixture types, since both components are fine in size, the overall particle sizes of the powder beds are fine for all APAP amounts. Reducing the overall particle size of the powder bed introduces a higher content uniformity discrepancy that can reach twice or even triple the average deviation in some proportions than those from mixtures containing at least one coarse component.
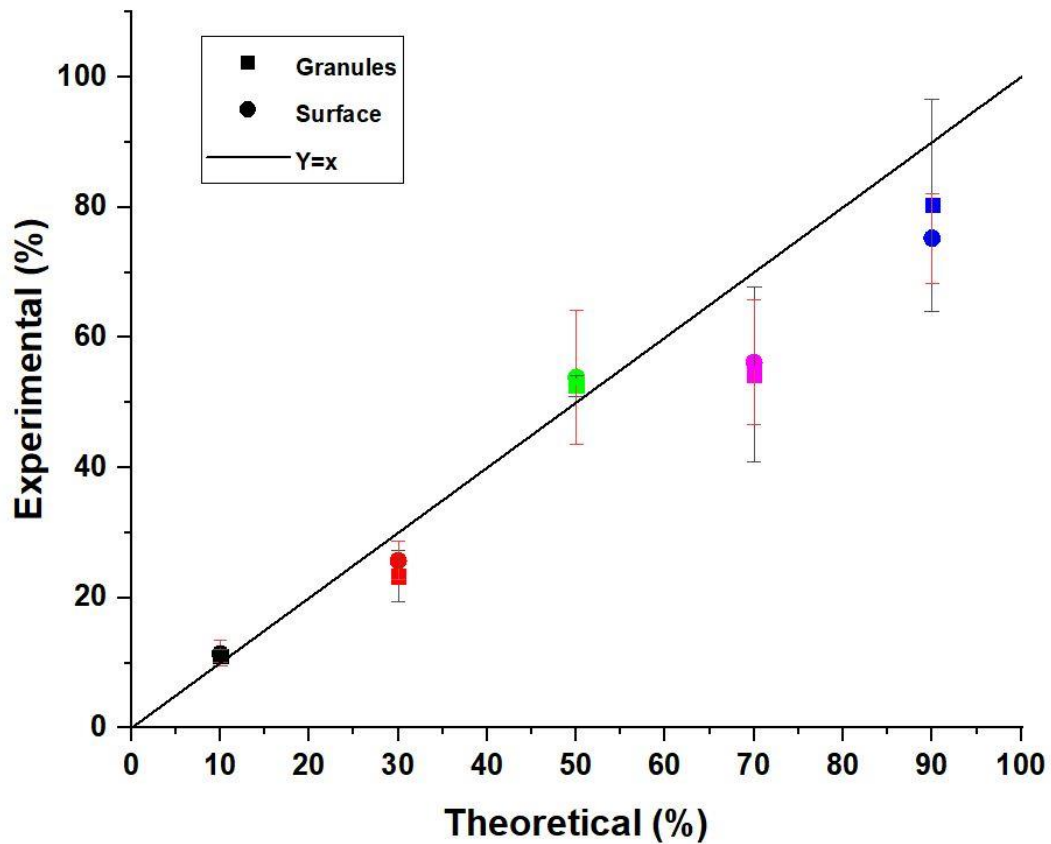
Figure 6.3 Composition of granules and powder bed surface containing different proportions of APAP with MCC from Fine-MCC/Fine-APAP mixtures.

Fine-MCC/ Fine-APAP	10 % (APAP)	30 %	50 %	70 %	90 %
Theoretical (% APAP)	10	30	50	70	90
Bed surface (% APAP)	11.5 ± 2.0	25.7 ± 3.0	53.9 ± 10.3	56.2 ± 9.6	75.3 ± 6.9
Average deviation in bed surface vs. theoretical (%)	2.6	5.6	8.7	17.5	16.1
Granules (% APAP)	11.1 ± 0.9	23.3 ± 3.9	52.6 ± 1.6	54.3 ± 13.5	80.3 ± 16.3
Average deviation in granules vs. theoretical (%)	1.5	6.0	3.0	21.3	19.2
Normalized API	0.97 ± 0.19	0.91 ± 0.18	0.98 ± 0.19	0.97 ± 0.29	1.07 ± 0.24

Table 6-3 Measured APAP weight percentage for each proportion in powder bed surface and granules from Fine-MCC/Fine-APAP mixtures (averages with standard deviations for two replicates for each mixture).

In Fine-MCC/Coarse-APAP mixtures, for the lower APAP amounts (10 % and 30 %), the content uniformities of both the bed surface and the granules from experiments are close to the theoretical values (see Fig. 6.4). With the increase of APAP, the content discrepancy between the bed surface and granules becomes larger, indicating the

preferential wetting effect. This discrepancy is reflected in the normalized API in Table 6-

4.
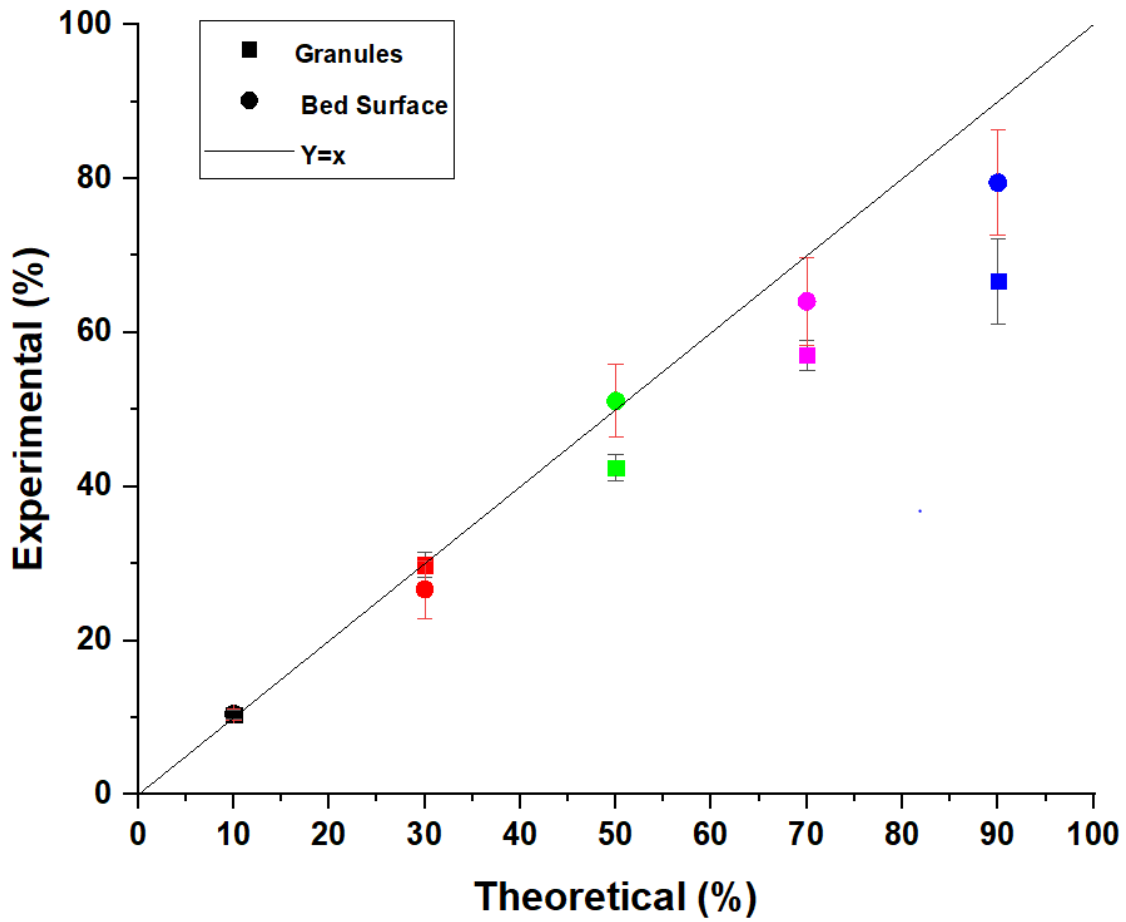
Figure 6.4 Composition of granules and powder bed surface containing different proportions of APAP with MCC from Fine-MCC/Coarse-APAP mixtures.

Fine-MCC/Coarse-APAP	10 % (APAP)	30 %	50 %	70 %	90 %
Theoretical (% APAP)	10	30	50	70	90

Bed surface (% APAP)	10.5 ± 0.8	26.7 ± 3.7	51.1 ± 4.7	64.1 ± 5.7	79.5 ± 6.8
Average deviation in bed surface vs. theoretical (%)	0.9	5.1	4.9	8.5	13
Granules (% APAP)	10.4 ± 0.5	29.8 ± 1.7	42.4 ± 1.7	57.1 ± 2.0	66.7 ± 5.6
Average deviation in granules vs. theoretical (%)	0.7	1.8	8.5	14.3	26.2
Normalized API (%)	0.99 ± 0.08	1.12 ± 0.17	0.83 ± 0.08	0.89 ± 0.09	0.84 ± 0.10

Table 6-4 Measured APAP weight percentage for each proportion in powder bed surface and granules from Fine-MCC/Coarse-APAP mixtures (averages with standard deviations for two replicates for each mixture).

From the results of four different mixture types (Coarse-MCC/Fine-APAP, Coarse-MCC/Coarse-APAP, Fine-APAP/Fine-APAP and Fine-MCC/Coarse-APAP), the following preliminary findings are concluded.

Both the mixture particle size distribution and the hydrophobicity have an impact on the content uniformity. for a small amount of APAP (10 %), the APAP content in both the granules and the bed surface are very uniform in all four mixture types, i.e., close to the theoretical values. In this proportion, since MCC dominates the mixture amount (90 %),

changing the particle size of MCC (hydrophilic component) will not have a significant effect on content uniformity. When the APAP amount increases above 30 %, for the two mixtures with Fine-APAP, the content uniformity starts to become compromised, and the content discrepancies reach the highest around 70 % and 80 % APAP. on the other hand, for coarse/coarse mixtures, the content uniformity is much less compromised for the same APAP proportions compared with the other two mixture types. The overall content of APAP is much more uniformly distributed in coarse powder mixtures than in fine powder mixtures. However, in fine powder mixtures, higher APAP amounts in the mixtures (higher mixture hydrophobicity) also cause a greater content discrepancy than lower APAP amounts (lower mixture hydrophobicity).

The difference between the content in the granules and that in the bed surface is represented by the normalized API percentage. Specifically, the APAP content in the granules is more compromised than that in the bed surface from the mixtures of Coarse-MCC/Fine-APAP (lowest normalized API % is 0.49) and Fine-MCC/Coarse-APAP (lowest normalized API % is 0.84), while in mixtures of Fine-MCC/Fine-APAP and Coarse-MCC/Coarse-APAP this difference is much smaller (lowest normalized API % is 0.91 and 0.93, respectively). The relationship between normalized API percentage and APAP proportions from all four mixtures were plotted in Fig 6.5. It is clear that when the APAP proportion is low (10 % and 30 %), the normalized API values are close to 100 %, meaning the APAP content in the granules are close to that in the bed surface in the same

proportion. When APAP increased above 30 %, the normalized API from Coarse/Fine and Fine/Coarse mixtures deviate more from 100 % compared with the other two (both Coarse and Fine) mixtures. This indicates the preferential wetting of ingredients for higher APAP proportions in those mixtures.
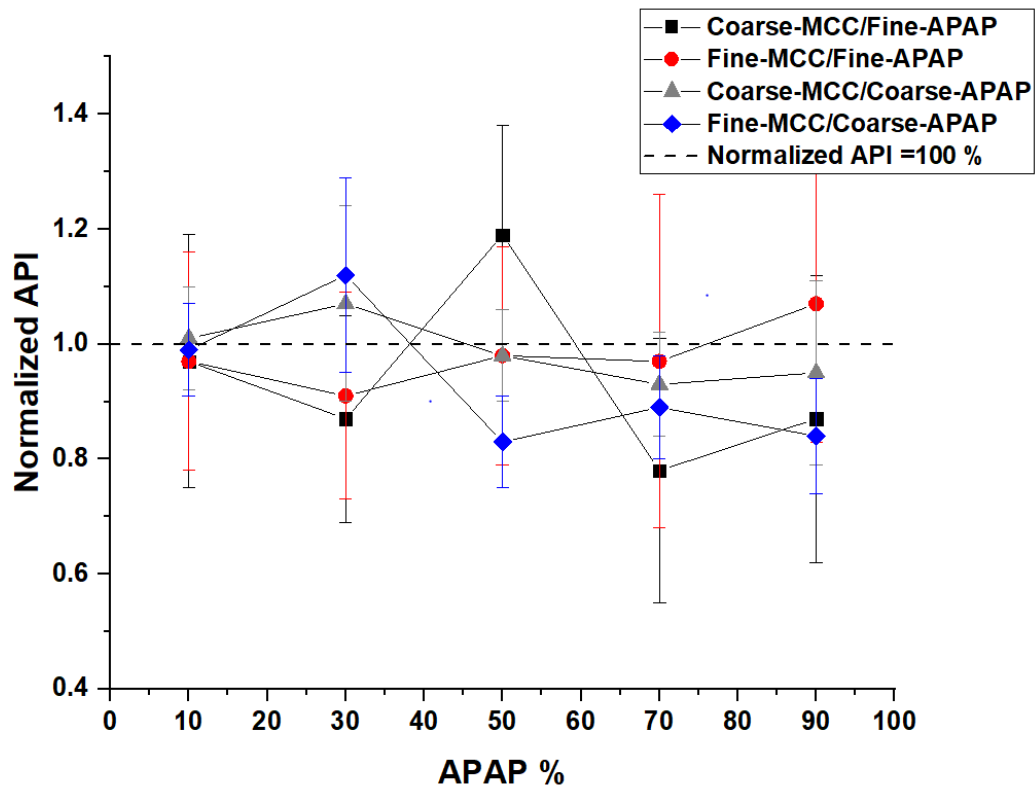
Figure 6.5 Normalized API percentage vs. APAP proportions for all mixtures.

Some hypotheses were also made based on the results. When the APAP proportion is low (i.e., low amount of the more hydrophobic component), the API content is uniform regardless of the different mixture types and particle sizes. When the APAP proportion is high (i.e., high amount of the more hydrophobic component), large differences between

87

the content in the bed surface and that in the granules exist in mixtures of Coarse-MCC/Fine-APAP and Fine-MCC/Coarse-APAP, while this difference is much smaller in the mixtures of Coarse-MCC/Coarse-APAP and Fine-MCC/Fine-APAP. Thus, it seems that preferential wetting of the MCC over APAP will occur when the differences in the particle sizes between MCC and APAP in the powder bed are large (i.e., the mixtures of one fine and one coarse ingredient).

The content uniformity results can be associated with the granule formation mechanisms (see Fig. 6.6). Generally, the formation mechanisms are affected directly by the overall bed particle size, while hydrophobicity has a minimal effect. Spreading occurred for coarse particle sizes, while Tunneling occurred for fine particle sizes. From the correlation plot between formation mechanisms and content uniformity variance (see Fig 6.6), it seems that there is no direct relationship. In either Tunneling or Spreading, both low and high variances of the content uniformity exist.
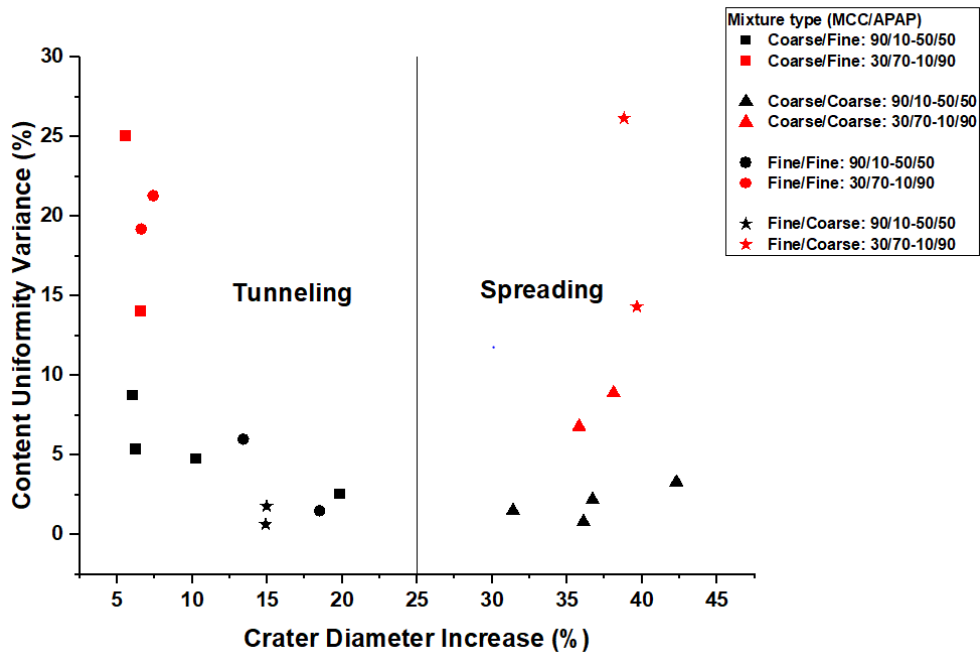
Figure 6.6 Relationship between granule formation mechanisms and content uniformity.

6.3.Conclusion

From this study of the content uniformity of APAP in both the granules formed and the powder bed surface, it is found that for lower APAP proportions (less than 50 %), the component contents are close to the theoretical values in all mixture types. When APAP proportions increase above 50 %, Coarse-MCC/Coarse-APAP mixtures show the most uniformity compared with the other three mixture types, where a sub-potent APAP trend is revealed in either the bed surface or granules.

The difference between the content in the granules and that in the bed surface is represented by the normalized API percentage (content in the granules divided by the

89

content in the bed surface). Specifically, the APAP content in the granules is more compromised than that in the bed surface from the mixtures of Coarse-MCC/Fine-APAP (lowest normalized API % is 0.49) and Fine-MCC/Coarse-APAP (lowest normalized API % is 0.84), while in mixtures of Fine-MCC/Fine-APAP and Coarse-MCC/Coarse-APAP, this difference is much smaller (lowest normalized API % is 0.91 and 0.93, respectively). The standard deviations among the replicates in the same proportion are much higher in the mixtures with high APAP proportions.

CHAPTER 7. GRANULE FORMATION REGIME MAP

7.1.Introduction

In this chapter, the relationship between granule formation mechanisms and powder mixture properties will be investigated, and formation regime maps for all four mixture types will be established and compared with the original regime map of single drop granulation on pure component powder beds [20]. The regime map analysis will help design and predict the process and products of wet granulation.

7.2.Granule formation mechanism regime map for powder mixtures

The original granule formation mechanism regime map dimensionless groups, bed porosity and Bond number, were calculated for each proportion in all four mixture types and compared to the corresponding formation mechanisms observed. Even though a modified Bond number, Bo_g^*, is defined in Equation 9 by Emady et al. [20] in Chapter 2, there are multiple versions of the Bond number that may be more applicable for single drop granulation. The Bond number was originally modified from Naze et al. [64], defined as:

$$Bo_g = \frac{\gamma}{d_{32}^2 \rho_p g} \tag{13}$$

which omitted the factor of contact angle ($cos\theta$). However, the determination of the contact angle is nontrivial. The contact angle of the two pure materials are based on literature values (see Chapter 3), but it is not clear if changing the particle size will affect the contact

angle. In our case, we assumed the contact angles of both materials with water to be fixed, regardless of different particle sizes. To investigate the influence of contact angle on Bond number, three different calculations were made: original Bond number (Bo_g) without contact angle, the Bond number (Bo_g*) defined in Eqn. (9), and the Bond number (Bo_g*^m). Bo_g*^m is introduced here as similar to Bo_g*, but with a modified $cos\theta$ calculated, based on the theory in Section 3.2.3. The mixture data, with bed porosity, Bond numbers and corresponding formation mechanisms from Coarse-MCC/Fine-APAP mixtures are given in Table 7-1. This data for the other three mixture types is given in Table 7-2.

Mixture type	Bo_g	Bo_g*	Bo_g*^m	Bed porosity	formation mechanism
C/F-100/0	3.96E3	3.21E3	3.21E3	0.79 ± 0.01	Spreading
C/F-90/10	4.69E3	3.42E3	3.44E3	0.82 ± 0.01	Spreading
C/F-80/20	5.62E3	3.66E3	3.58E3	0.83 ± 0.01	Spreading
C/F-75/25	6.18E3	3.78E3	3.59E3	0.85 ± 0.01	Spreading/Tunneling
C/F-70/30	6.83E3	3.90E3	3.52E3	0.85 ± 0.01	Spreading/Tunneling
C/F-65/35	7.58E3	4.03E3	3.34E3	0.86 ± 0.01	Spreading/Tunneling
C/F-60/40	8.45E3	4.16E3	2.97E3	0.87 ± 0.01	Spreading/Tunneling
C/F-50/50	1.07E4	4.40E3	1.32E3	0.87 ± 0.01	Tunneling
C/F-40/60	1.38E4	4.61E3	2.4E2	0.88 ± 0.01	Tunneling
C/F-30/70	1.84E4	4.69E3	3.2E2	0.88 ± 0.01	Tunneling
C/F-20/80	2.56E4	4.50E3	4.5E2	0.91 ± 0.01	Tunneling
C/F-10/90	3.77E4	3.64E3	6.57E2	0.91 ± 0.01	Tunneling
C/F-0/100	6.00E4	1.05E3	1.05E3	0.89 ± 0.01	Tunneling

Table 7-1 Bond number, bed porosity, and formation mechanism for Coarse-MCC/Fine-APAP mixtures.

.

Mixture type	Bo_g	Bo_g*	Bo_g*^m	Bed porosity	formation mechanism
C/C-90/10	3.76E3	2.75E3	3.04E3	0.79 ± 0.01	Spreading
C/C -80/20	3.58E3	2.33E3	2.90E3	0.78 ± 0.01	Spreading
C/C -75/25	3.50E3	2.14E3	2.83E3	0.77 ± 0.01	Spreading
C/C -70/30	3.42E3	19571E3	2.22E3	0.76 ± 0.01	Spreading
C/C -50/50	3.15E3	1.30E3	9.08E2	0.75 ± 0.01	Spreading
C/C -30/70	2.93E3	7.46E2	3.91E2	0.74 ± 0.01	Spreading
C/C -10/90	2.75E3	2.65E2	1.31E2	0.73 ± 0.01	Spreading
F/F-90/10	1.97E4	1.44E4	1.53E4	0.86 ± 0.01	Tunneling
F/F-70/30	2.46E4	1.41E4	1.65E4	0.87 ± 0.01	Tunneling
F/F-50/50	3.12E4	1.29E4	1.52E4	0.87 ± 0.01	Tunneling
F/F-30/70	4.06E4	1.03E4	2.22E3	0.87 ± 0.01	Tunneling
F/F-10/90	5.42E4	5.24E3	9.47E2	0.88 ± 0.01	Tunneling
F/C-90/10	1.28E4	9.36E3	1.04E4	0.85 ± 0.01	Spreading/Tunneling
F/C-70/30	7.69E3	4.39E3	4.99E3	0.82 ± 0.01	Spreading/Tunneling
F/C-50/50	5.21E3	2.15E3	1.50E3	0.79 ± 0.01	Spreading
F/C-30/70	3.83E3	9.76E2	5.12E2	0.76 ± 0.01	Spreading
F/C-10/90	2.98E3	2.88E2	1.42E2	0.74 ± 0.01	Spreading

Table 7-2 Bond number, bed porosity, and formation mechanism for Coarse-MCC/Coarse-APAP, Fine-MCC/Fine-APAP, and Fine-MCC/Coarse-APAP mixtures.

The regime map with the relationship between the bed porosity and the original Bond

number Bo_g of all four mixture types is shown in Fig 7.1. The data follow a similar trend

in all four mixtures. Tunneling occurs at high values of Bo_g, with values ranging from 1.06E4 to 6.00E4. on the other hand, Spreading occurs at low values of Bo_g, with values ranging from 2.45E3 to 5.62E3. There is a narrow area of transition from Spreading to Tunneling from 6.18E3 to 1.06E4.

Figure 7.1 Regime map of Bond number Bo_g vs. bed porosity for all four mixtures. (Fully filled points indicate the Spreading, partially filled points indicate Transition and open points indicate Tunneling.)

The regime map with the relationship between the bed porosity and the Bond number Bo_g* with the factor of the original contact angle using Cassie-Baxter theory is shown in

Fig 7.2. The regime map with the modified Bond number Bo_g*^m with the modified contact

angle is shown in Fig 7.3. for the regime map with Bo_g*, with the increase of Bond number,

a trend similar to that in Fig. 7.1 was observed, where Spreading occurred with small Bond

numbers and Tunneling occurred with large Bond numbers. However, there are couple of

Tunneling points where the Bond numbers are smaller than those from the

Spreading/Tunneling transition. Based on the Bond number equation (Eqn. (9)), the contact

angle is in the numerator, while the particle size is in denominator. for Coarse-MCC/Fine-

APAP mixtures, when the APAP proportion increases above 60 %, the contact angle values

descend much faster than the particle size, leading to a sharp drop in the Bond number.

This trend is even apparent for the modified Bond number, $Bo*^m$, where f, the calculated

volume fraction of APAP in Eqn. (10), is equal to 100 % for batches with real APAP

proportions from 60 % to 100 % (shown in Fig. 7.3). Thus, the modified $cos\theta$ values are

all 0.017 ($\theta = 90°$) for those proportions, rather than the values gradually decreasing. The

Tunneling points that fall into small Bond number ranges are all from Coarse-MCC/Fine-

APAP mixtures.

for the other three mixture types, the similar trend of Bond number values was

observed; however, the reverse (increase and then drop) effect is much less compared with

that in Coarse-MCC/Fine-APAP mixtures. Most of the Spreading points fall into lower

values, while the Tunneling points fall into higher values. only a couple of the Tunneling

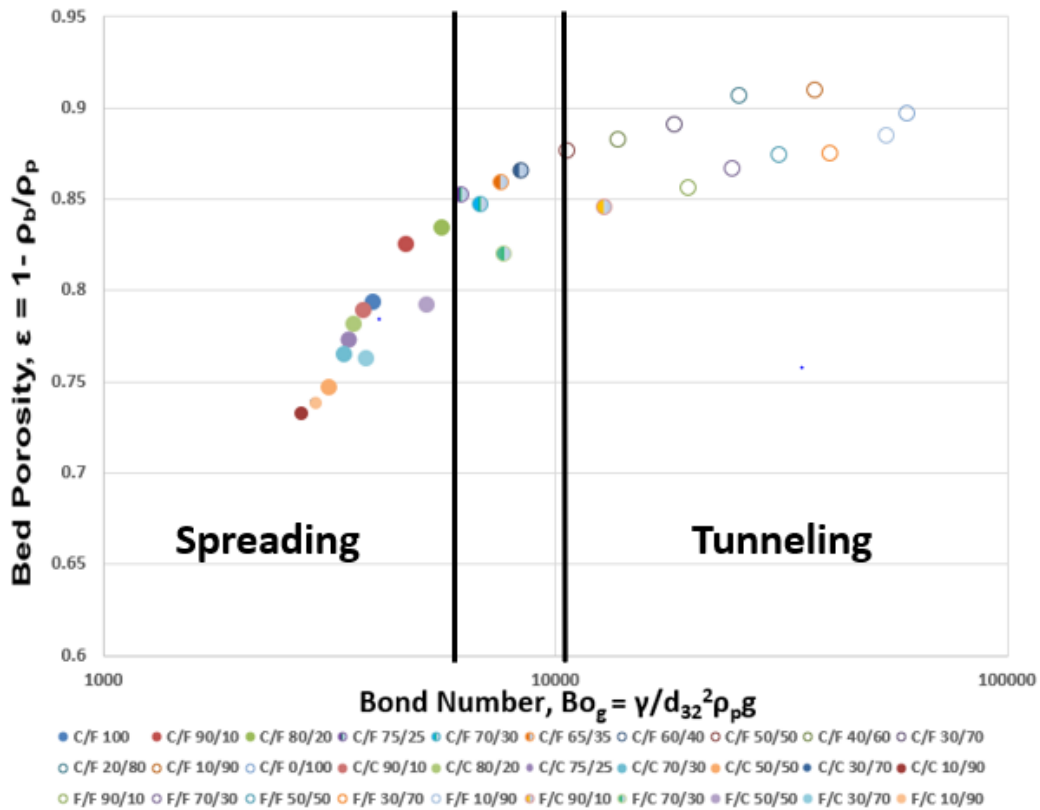points have low Bond numbers, due to the sharp decrease in $cos\theta$.
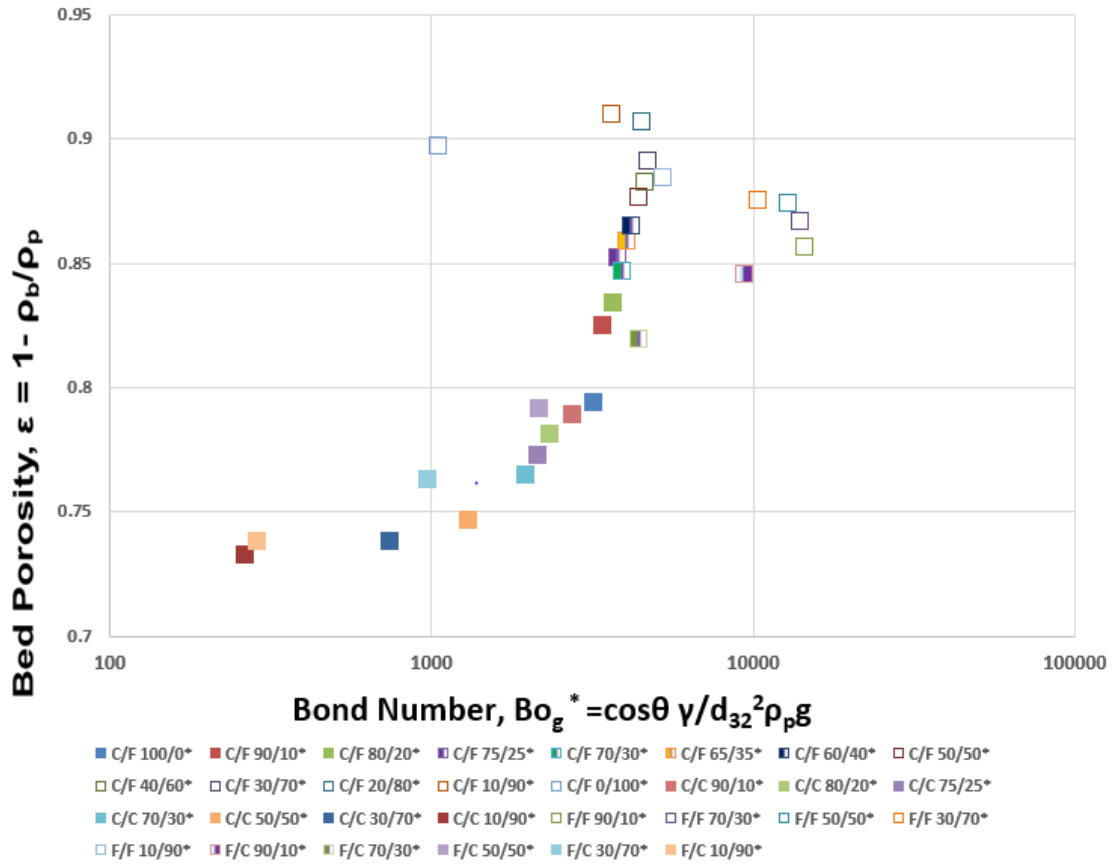
Figure 7.2 Regime map of Bond number Bo$_g$* vs bed porosity for all four mixtures. (Fully filled points indicate the Spreading, partially filled points indicate Transition and open points indicate Tunneling.)
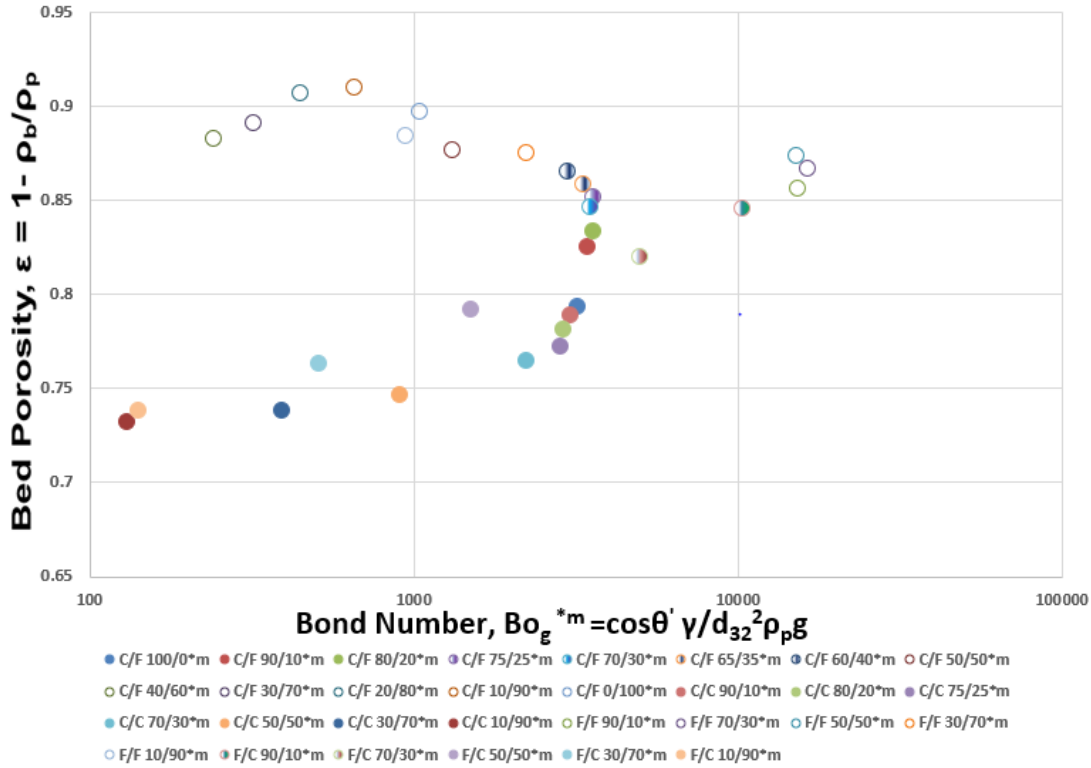
Figure 7.3 Regime map of Bond number Bo_g*^m *modified* vs bed porosity for all four mixtures. (Fully filled points indicate the Spreading, partially filled points indicate Transition and open points indicate Tunneling.)

7.3. Regime Map Comparison with Literature

The granule formation mechanism regime map from the literature, for single drop granulation on pure component powder beds, was shown in Fig. 2.4. The Bond number boundary is 65000, where Tunneling occurs when $Bo_g^* > 65000$ and Spreading occurs when $Bo_g^* < 65000$. This regime map took the factor of contact angle into consideration. However, since most available literature data did not have contact angle measurements, a regime map that did not include the contact angle was also established, using Bo_g rather than Bo_g^* [20]. Here, a similar distribution of the data was observed; however, the transition

boundary was much larger ($Bo_g \approx 1.0E5$). To compare the formation mechanisms of binary

mixtures from this dissertation with the pure components available in the literature, the

Bo_g regime map (without contact angle) is shown in Fig. 7.4, with an added boundary range

that considers the results from the present work.
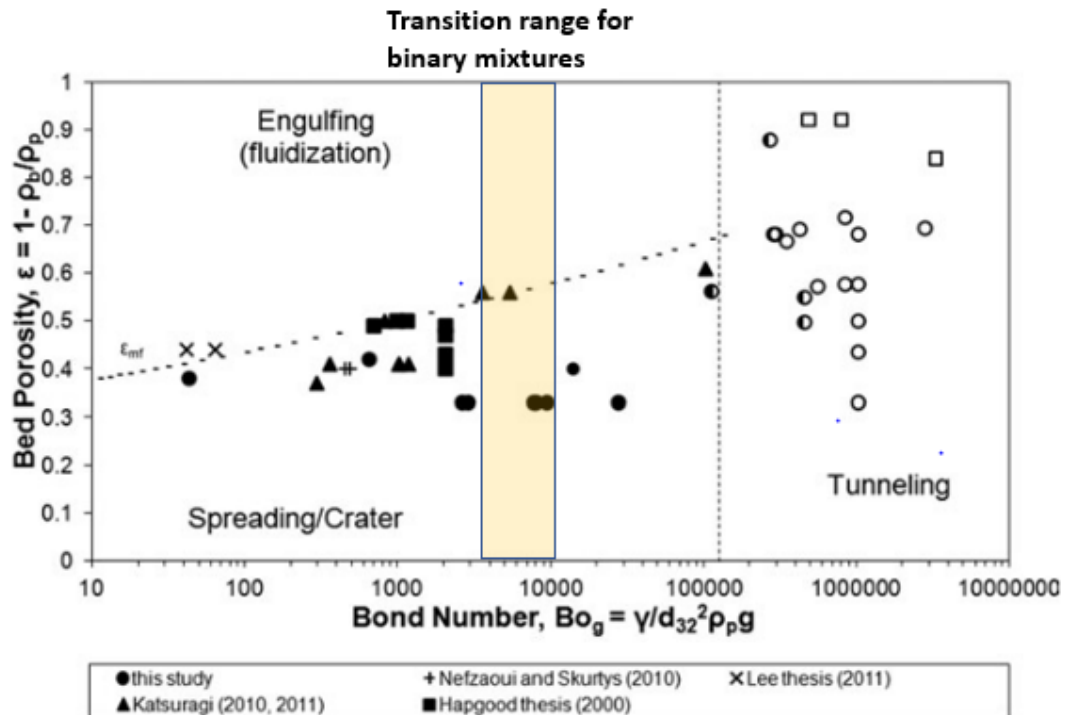
Figure 7.4 Regime map of the Bond number without the factor of contact angle [20] (the partially transparent region is the transition range for binary mixtures from this work).

The formation mechanism transition boundary is $Bo_g \approx 1.05E5$ for single drop

granulation on pure component powder beds (see Fig. 7.4). Compared with the single drop

granulation on binary mixtures in this work, where the transition area ranges from 5.21E3

to 1.28E4 (shown in the yellow partially filled region in Fig. 7.4), the original boundary is

much further to the right. The transition range for binary mixtures completely falls into the Spreading region for pure component powder beds. The reason for this discrepancy requires further investigation.

7.4.Relationship between Granule Morphology and formation Mechanisms

Besides the regime map, the relationships between the granule morphology and formation mechanisms were also previously investigated for pure components [20], represented by *V.A.R.* vs. Bo_g^*. Based on the results from Emady et al., *V.A.R.* was not a function of Bo_g^* for the Tunneling mechanism. In the four binary mixtures in the present study, to revise the relationship between granule morphology and formation mechanisms, the Bond number was replaced by the crater diameter increase, which is a direct reflection of the formation mechanism (see Chapter 4). From the new relationship (see Fig 7.5), it can be seen that with the increase of crater diameter increase, the V.A.R. value increases as well. With a crater diameter increase less than 15 %, Tunneling occurs, and the V.A.R. ranges from 1.23 to 1.52. The Spreading/Tunneling transition occurs where the crater diameter increase is from 15 % to 24 %, where the V.A.R. values increase with a range from 1.24 to 2.21. Spreading occurs where the crater diameter increase is greater than 35 %, and the V.A.R values range from 1.79 to 3.09. Thus, the V.A.R has a linear relationship with the crater diameter increase. When Tunneling occurs (low crater diameter increase), the granules are more spherical with small V.A.R. values, while when Spreading occurs (high crater diameter increase), the granules are plate-like with larger V.A.R. values.

99
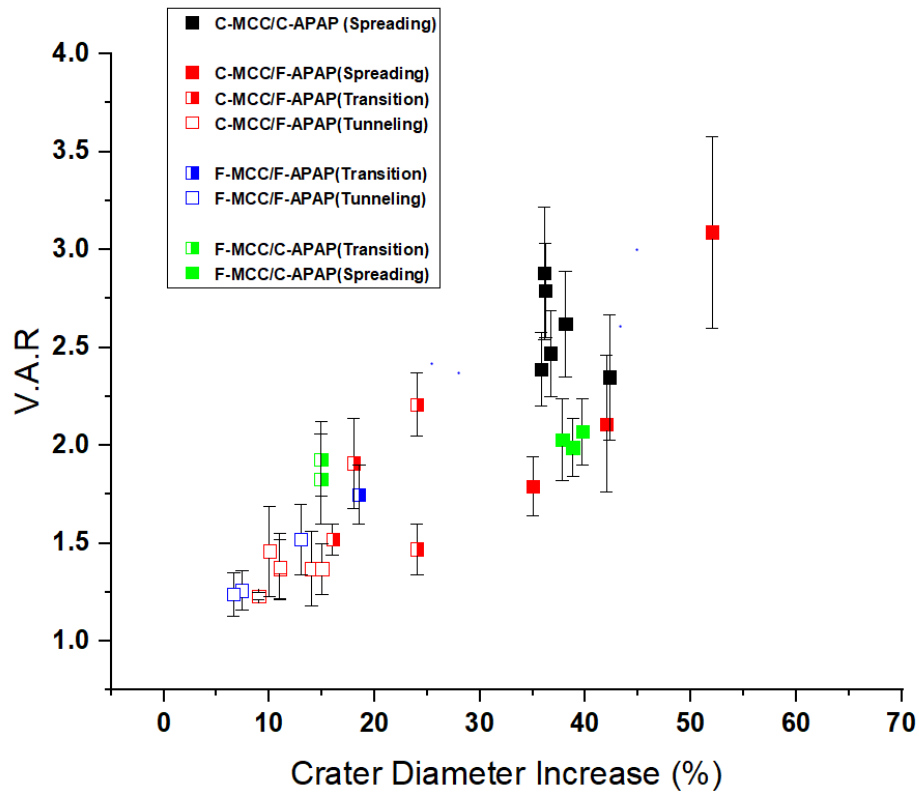
Figure 7.5 Regime map of granule morphology (indicated by *V.A.R.*) vs. formation mechanism (indicated by the crater diameter increase).

7.5.Conclusion

The granule formation mechanism regime maps for binary mixtures were established in this chapter. The Bond number Bo_g and crater diameter increase were used as the indicators for determining the formation mechanism The Bond number with and without the contact angle factor, *cosθ*, were both investigated. It was found that the Bond number without the contact angle factor was a better indicator of formation mechanism, and it shows a similar trend to that for pure component powder beds [20]. Additionally, the

relationship between the granule morphology and formation mechanism was also studied. Generally, with the increase of crater diameter increase (indicating the transition from Tunneling to Spreading), the V.A.R.'s of the granules increased as well (granules turn from round to plate-like). The regime maps can be used to predict the granule formation mechanism as well as the general granule morphology. However, there is still room for improvement in refining the factors that determine the Bond number.

CHAPTER 8. CONCLUSIONS AND FUTURE WORK

8.1.Conclusions

The primary objective of this dissertation was to investigate the mechanisms of single drop impact onto static powder beds of binary mixtures, and the formed granule properties. Two kinds of pharmaceutical materials, microcrystalline cellulose (MCC) and acetaminophen (APAP), with coarse and fine sizes for both components, were used to make powder beds. Thus, four mixture types were made based on the combinations of the two materials, each with two different particle sizes.

Drop penetration time was measured for all mixtures. It was found that with the increase of APAP proportion in the mixtures, drop penetration time increased. Additionally, the penetration times in Coarse-MCC/Fine-APAP, Fine-APAP/Fine-APAP and Fine-MCC/Coarse-APAP were much longer than that in Coarse-MCC/Coarse-APAP. This reveals that the drop penetration times in mixtures with fine components are longer, indicating the influence of both particle size and hydrophobicity on penetration time.

Two different formation mechanisms were identified:

- **Tunneling**, in which particle aggregates were sucked into the drop, which tunneled into the powder bed during the penetration. This occurred in mixtures with fine particles. Specifically, it occurred in all proportions from Fine-MCC/Fine-APAP

mixtures and in APAP proportions from 50 % to 100 % from Coarse-MCC/Fine-APAP mixtures (with crater diameter increase smaller than 15 %).

- **Spreading**, in which the drop spread and then penetrated into the powder bed voids via capillary force. This occurred in mixtures with coarse particles. Specifically, it occurred in all proportions from Coarse-MCC/Coarse-APAP mixtures, APAP proportions from 0 % to 25 % from Coarse-MCC/Fine-APAP mixtures, and 50 % to 90 % from Fine-MCC/Coarse-APAP mixtures (with crater diameter increase greater than 35 %).

Granules formed were observed to have different shapes. The vertical aspect ratio (V.A.R.) was used as the measure of granule morphology, with value close to 1 indicating a perfectly spherical shape. The Tunneling mechanism produced round granules, with V.A.R.'s from 1.24 to 1.75. The Spreading mechanism produced flat disks, with V.A.R.'s from 2.07 to 3.1. The Spreading/Tunneling transition produced granules with shapes that were hybrids of the two mechanisms (V.A.R.'s from 1.52 to 2.21).

The internal structure of the bed surface and the granules from Coarse-MCC/Fine-APAP were studied via micro-CT scanning. The porosities of the granules produced from the Spreading mechanism were higher than those of the granules produced from the Tunneling mechanism. With the increase of the amount of APAP, the granules made from heterogeneous mixtures became more complex, especially for those in the transitional

regime that exhibited characteristics of both Spreading and Tunneling, where the internal structure was relatively non-uniform, containing both dense and loose regions.

The content uniformity of the bed surface and the granules from all mixtures were investigated via UV-Vis spectrometry. for lower APAP proportions (less than 50 %), the content of APAP from both the granules and the bed surfaces were uniform for all mixture types. for higher APAP proportions, the content was compromised, especially for Coarse/Fine, Fine/Fine and Fine/Coarse mixtures. The discrepancy between the content in the bed surface and the granules was larger for Coarse-MCC/Fine-APAP and Fine-MCC/Coarse-APAP mixtures, indicating the preferential wetting for those mixtures where the components were of different particle sizes.

The granule formation mechanism regime maps revealed that the formation mechanisms were determined by the Bond number, Bo_g, as previously demonstrated for single component materials [20]. Tunneling occurred for Bo_g>1.06E4, while Spreading occurred for Bo_g<5.62E3. The Tunneling/Spreading transition occurred for a Bo_g range in the range of 5.62E3 to 1.06E4. Additionally, the relationship between granule morphology and formation mechanisms showed that when the formation mechanism transitioned from Tunneling to Spreading, the V.A.R. of the granules increased as well (granules turned from round to plate-like). Using the granule formation regime maps, the formation mechanism along with general granule shape can be predicted.

This was the first study to relate drop penetration time, granule formation mechanisms, granule morphology and internal structure to the particle size and hydrophobicity in drop-controlled granulation for binary mixtures. Additionally, regime maps were presented to predict the formation mechanism and general granule shape for these materials, extending the applicability of the previously developed regime maps [20]. The results have significant impact on the design and prediction of single drop wet granulation, which can now be extended to more complex systems.

8.2.Future Work

The following is a list of proposed future work:

1) Optimize the formation mechanism regime maps for single drop granulation on heterogeneous beds.

Regime maps for single drop granulation on heterogeneous beds have been established to predict the formation mechanisms and granule morphology in Chapter 7, based on particle size distribution and bed porosity. However, this is still a preliminary result due to the complexity of the contact angles of particle mixtures. To optimize the regime map to better examine the effect of contact angle, binary mixtures containing components with similar

contact angles (of separately high and low contact angles) are also recommended to contrast with the MCC/APAP mixtures.

2) Establish a single drop granulation model, based on discrete element method simulations.

Few studies of model-based simulation have been conducted on wet granulation, let alone on single drop granulation. Establishing models would help in understanding the fundamental mechanisms of wet granulation. Furthering the knowledge of how a drop interacts with a powder bed is necessary to predict and design granulation processes. The preliminary model will be set up for single drop granulation on the simplest mono-component case. The simulated granulation processes with different crater diameter increases will be compared to identify Tunneling vs. Spreading. once the model is validated with appropriate parameters, more complicated cases would be tested.

3) Perform high shear granulation on single component materials of both fine and coarse particle sizes and compare the results with single drop granulation.

Even though single drop wet granulation was studied for a binary mixture, high shear granulation is still a commonly used process method in many industries. Thus, it is essential to study the translation of the single drop granulation results to practical granulation processes. The same materials and similar proportions will be used for high shear granulation. Additionally, similar drop conditions like drop size and drop height from

single drop granulation will be applied. The granule properties like morphology, size and content uniformity will be characterized to compare the two granulation methods.

4) Study the effect of smaller liquid drop size and alternative measurement of particle size distribution.

So far, the liquid binder used was DI water, and the drop size was standardized from a gauge 22 syringe needle. It is assumed that changing the liquid drop size should also affect the granulation, especially when the drop size is reduced to the level of the particle size of the powder material. Thus, different drop sizes will be used for conducting single drop impact experiments, and compared with the previous results. Additionally, the current particle size distribution measurement is based on the surface mean (d_{32}), which we believe to be the most relevant parameter for granulation processes. However, there are still potential alternative measurements that can be compared in calculating the Bond number to optimize the regime map.

5) Study the component distribution of the internal structure using micro-CT.

The internal structure of the granules and powder bed were investigated using micro-CT. However, due to the limitation of micro-CT, it was impossible to distinguish the distribution of binary components with same phase (in our case, both were organic materials). Thus, powder materials with different component phases, like metallic/organic, will be used and applied to micro-CT scanning for spatial distribution studies.

6) Establish drop penetration time regime map and compared with literature work

As mentioned in Chapter 2.2, even though the drop penetration time was studied thoroughly for different complicated mixtures by previous researchers, the current model did not fit the experimental results very well, especially those with hydrophobic materials. The measured drop penetration time of single drop granulation from all four mixtures will be compared with the theoretical time calculated based on Eqn. (6) to validate the model.

REFERENCES

[1]   K.P. Hapgood, J.D. Litster, S.R. Biggs, T. Howes, Drop Penetration into Porous Powder Beds, J. Colloid Interface Sci. 253 (2002) 353–366. https://doi.org/10.1006/jcis.2002.8527.

[2]   J.D. Litster, K.P. Hapgood, J.N. Michaels, A. Sims, M. Roberts, S.K. Kameneni, T. Hsu, Liquid distribution in wet granulation: Dimensionless spray flux, Powder Technol. 114 (2001) 32–39. https://doi.org/10.1016/S0032-5910(00)00259-X.

[3]   S.M. Iveson, J.D. Litster, K. Hapgood, B.J. Ennis, Nucleation, growth and breakage phenomena in agitated wet granulation processes: A review, Powder Technol. 117 (2001) 3–39. https://doi.org/10.1016/S0032-5910(01)00313-8.

[4]   J. Lister, B. Ennis, The Science and Engineering of Granulation Process, Dordr. ; Boston, Mass. Kluwer Acad. Publ. (2004).

[5]   S. Middleman, Modeling axisymmetric flows: dynamics of films, jets, and drops, Academic Press, 1995.

[6]   A. Marmur, The radial capillary, J. Colloid Interface Sci. 124 (1988) 301–308. https://doi.org/10.1016/0021-9797(88)90351-7.

[7]   M. Denesuk, G.L. Smith, B.J.J. Zelinski, N.J. Kreidl, D.R. Uhlmann, Capillary penetration of liquid droplets into porous materials, J. Colloid Interface Sci. 158 (1993) 114–120. https://doi.org/10.1006/jcis.1993.1235.

[8]   T. Nguyen, W. Shen, K. Hapgood, Drop penetration time in heterogeneous powder beds, Chem. Eng. Sci. 64 (2009) 5210–5221. https://doi.org/10.1016/j.ces.2009.08.038.

[9]   D. Kayrak-Talay, S. Dale, C. Wassgren, J. Litster, Quality by design for wet granulation in pharmaceutical processing: Assessing models for a priori design and scaling, Powder Technol. 240 (2013) 7–18. https://doi.org/10.1016/j.powtec.2012.07.013.

[10]   M.L.M. Oostveen, G.M.H. Meesters, J.R. van Ommen, Quantification of powder wetting by drop penetration time, Powder Technol. 274 (2015) 62–66. https://doi.org/10.1016/j.powtec.2014.09.021.

[11]   C.P. Whitby, X. Bian, R. Sedev, Spontaneous liquid marble formation on packed porous beds, Soft Matter. 44 (2012) 11336–11342. https://doi.org/10.1039/c2sm26529j.

[12]   C.P. Whitby, X. Bian, R. Sedev, Rolling, penetration and evaporation of alcohol-

water drops on coarse and fine hydrophobic powders, Colloids Surfaces A Physicochem. Eng. Asp. 436 (2013) 639–649. https://doi.org/10.1016/j.colsurfa.2013.07.041.

[13] J.O. Marston, J.E. Sprittles, Y. Zhu, E.Q. Li, I.U. Vakarelski, S.T. Thoroddsen, Drop spreading and penetration into pre-wetted powders, Powder Technol. 239 (2013) 128–136. https://doi.org/10.1016/j.powtec.2013.01.062.

[14] H.R. Charles-Williams, R. Wengeler, K. Flore, H. Feise, M.J. Hounslow, A.D. Salman, Granule nucleation and growth : Competing drop spreading and in fi ltration processes, Powder Technol. 206 (2011) 63–71. https://doi.org/10.1016/j.powtec.2010.06.013.

[15] H. Charles-Williams, R. Wegeler, K. Flnore, H. Feise, M.J. Hounslow, A.D. Salman, Granulation behaviour of increasingly hydrophobic mixtures, Powder Technol. 238 (2013) 64–76. https://doi.org/10.1016/j.powtec.2012.06.009.

[16] S.-C. Zhao, R. de Jong, D. van der Meer, Liquid-grain mixing suppresses droplet spreading and splashing during impact, (2016). http://arxiv.org/abs/1607.00285.

[17] T. Supakar, M. Moradiafrapoli, G.F. Christopher, J.O. Marston, Spreading, encapsulation and transition to arrested shapes during drop impact onto hydrophobic powders, J. Colloid Interface Sci. 468 (2016) 10–20. https://doi.org/10.1016/j.jcis.2016.01.028.

[18] A.A.P. Kumar, V.P. Sandireddy, T. Banerjee, D. Bandyopadhyay, Dynamics of a liquid droplet on a granular bed of microstructured particles: From lens formation to marble effect, Ind. Eng. Chem. Res. 54 (2015) 1131–1141. https://doi.org/10.1021/ie5024904.

[19] K.P. Hapgood, B. Khanmohammadi, Granulation of hydrophobic powders, Powder Technol. 189 (2009) 253–262. https://doi.org/10.1016/j.powtec.2008.04.033.

[20] H.N. Emady, D. Kayrak-Talay, J.D. Litster, A Regime Map for Granule formation by Drop Impact on Powder Beds, AICHE. 7 (2013) 405–410. https://doi.org/10.1002/aic.

[21] H.N. Emady, D. Kayrak-Talay, W.C. Schwerin, J.D. Litster, Granule formation mechanisms and morphology from single drop impact on powder beds, Powder Technol. 212 (2011) 69–79. https://doi.org/10.1016/j.powtec.2011.04.030.

[22] R. Zhao, Q. Zhang, H. Tjugito, X. Cheng, Granular impact cratering by liquid drops: Understanding raindrop imprints through an analogy to asteroid strikes., Proc. Natl. Acad. Sci. U. S. A. 112 (2015) 342–7. https://doi.org/10.1073/pnas.1419271112.

[23] Q. Zhang, M. Gao, R. Zhao, X. Cheng, Scaling of liquid-drop impact craters in wet

granular media, Phys. Rev. E - Stat. Nonlinear, Soft Matter Phys. 92 (2015) 1–8. https://doi.org/10.1103/PhysRevE.92.042205.

[24] R. De Jong, S.C. Zhao, D. Van Der Meer, Crater formation during raindrop impact on sand, Phys. Rev. E. 95 (2017). https://doi.org/10.1103/PhysRevE.95.042901.

[25] R. Zhao, Q. Zhang, H. Tjugito, X. Cheng, Raindrop impact on a sandy surface, Phys. Fluids. 27 (2015) 2015–2017. https://doi.org/10.1063/1.4930917.

[26] S.-C. Zhao, R. de Jong, D. van der Meer, Raindrop impact on sand: a dynamic explanation of crater morphologies, Soft Matter. 11 (2015) 6529–6718. https://doi.org/10.1039/C5SM00957J.

[27] A.L. Mundozah, J.J. Cartwright, C.C. Tridon, M.J. Hounslow, A.D. Salman, Hydrophobic/hydrophilic static powder beds: Competing horizontal spreading and vertical imbibition mechanisms of a single droplet, Powder Technol. 330 (2018) 275–283. https://doi.org/10.1016/j.powtec.2018.02.032.

[28] D. van der Meer, Impact on Granular Beds, Annu. Rev. Fluid Mech. 49 (2017) 463–484. https://doi.org/10.1146/annurev-fluid-010816-060213.

[29] L. Farber, G. Tardos, J.N. Michaels, Use of X-ray tomography to study the porosity and morphology of granules, (n.d.). https://doi.org/10.1016/S0032-5910(03)00043-3.

[30] K.P. Hapgood, L. Farber, J.N. Michaels, Agglomeration of hydrophobic powders via solid spreading nucleation, Powder Technol. 188 (2009) 248–254. https://doi.org/10.1016/j.powtec.2008.05.004.

[31] N. Rahmanian, M. Ghadiri, X. Jia, F. Stepanek, Characterisation of granule structure and strength made in a high shear granulator, Powder Technol. 192 (2009) 184–194. https://doi.org/10.1016/j.powtec.2008.12.016.

[32] P. Kulinowski, K. Woyna-Orlewicz, J. Obrał, G.M. Rappen, D. Haznar-Garbacz, W.P. Węglarz, R. Jachowicz, G. Wyszogrodzka, J. Klaja, P.P. Dorozyński, Multimodal approach to characterization of hydrophilic matrices manufactured by wet and dry granulation or direct compression methods, Int. J. Pharm. 499 (2016) 263–270. https://doi.org/10.1016/j.ijpharm.2015.12.067.

[33] O. Kašpar, V. Tokárová, S. Oka, K. Sowrirajan, R. Ramachandran, F. Štěpánek, Combined UV/vis and micro-tomography investigation of acetaminophen dissolution from granules, Int. J. Pharm. 458 (2013) 272–281. https://doi.org/10.1016/j.ijpharm.2013.10.032.

[34] S. Dale, C. Wassgren, J. Litster, Measuring granule phase volume distributions using X-ray microtomography, Powder Technol. 264 (2014) 550–560.

https://doi.org/10.1016/j.powtec.2014.06.009.

[35] I. Hafsa, B. Cuq, S.J. Kim, A. Le Bail, T. Ruiz, S. Chevallier, Description of internal microstructure of agglomerated cereal powders using X-ray microtomography to study of process-structure relationships, Powder Technol. 256 (2014) 512–521. https://doi.org/10.1016/j.powtec.2014.01.073.

[36] R. Pashminehazar, A. Kharaghani, E. Tsotsas, Three dimensional characterization of morphology and internal structure of soft material agglomerates produced in spray fluidized bed by X-ray tomography, Powder Technol. 300 (2016) 46–60. https://doi.org/10.1016/j.powtec.2016.03.053.

[37] N.B. Davis, K. Waibel, K. Wang, J.D. Litster, Microstructure of single-droplet granules formed from ultra-fine powders, Powder Technol. 305 (2017) 19–26. https://doi.org/10.1016/j.powtec.2016.09.033.

[38] C. Li, N. Zhu, H.N. Emady, L. Zhang, Synchrotron-based X-ray in-situ imaging techniques for advancing the understanding of pharmaceutical granulation, Int. J. Pharm. (2019) 118797. https://doi.org/10.1016/j.ijpharm.2019.118797.

[39] M.X.L. Tan, T.H. Nguyen, K.P. Hapgood, Drug distribution in wet granulation: Foam versus spray, Drug Dev. Ind. Pharm. 39 (2013) 1389–1400. https://doi.org/10.3109/03639045.2012.719233.

[40] T.H. Nguyen, W. Shen, K. Hapgood, Effect of formulation hydrophobicity on drug distribution in wet granulation, Chem. Eng. J. 164 (2010) 330–339. https://doi.org/10.1016/j.cej.2010.05.008.

[41] S. Oka, D. Smrčka, A. Kataria, H. Emady, F. Muzzio, F. Štepánek, R. Ramachandran, Analysis of the origins of content non-uniformity in high-shear wet granulation, Int. J. Pharm. 528 (2017) 578–585. https://doi.org/10.1016/j.ijpharm.2017.06.034.

[42] S. Oka, H. Emady, O. Kašpar, V. Tokárová, F. Muzzio, F. Štěpánek, R. Ramachandran, The effects of improper mixing and preferential wetting of active and excipient ingredients on content uniformity in high shear wet granulation, Powder Technol. 278 (2015) 266–277. https://doi.org/10.1016/j.powtec.2015.03.018.

[43] H. Li, M.R. Thompson, K.P. O'Donnell, Examining drug hydrophobicity in continuous wet granulation within a twin screw extruder, Int. J. Pharm. 496 (2015) 3–11. https://doi.org/10.1016/j.ijpharm.2015.07.070.

[44] G.M. Mahours, D.E.Z. Shaaban, G.A. Shazly, S.H. Auda, The effect of binder concentration and dry mixing time on granules, tablet characteristics and content

uniformity of low dose drug in high shear wet granulation, J. Drug Deliv. Sci. Technol. 39 (2017) 192–199. https://doi.org/10.1016/j.jddst.2017.03.014.

[45]   S. Oka, O. Kašpar, V. Tokárová, K. Sowrirajan, H. Wu, M. Khan, F. Muzzio, F. Štěpánek, R. Ramachandran, A quantitative study of the effect of process parameters on key granule characteristics in a high shear wet granulation process involving a two component pharmaceutical blend, Adv. Powder Technol. 26 (2015) 315–322. https://doi.org/10.1016/j.apt.2014.10.012.

[46]   A. Kataria, S. Oka, D. Smrčka, Z. Grof, F. Štěpánek, R. Ramachandran, A quantitative analysis of drug migration during granule drying, Chem. Eng. Res. Des. 136 (2018) 199–206. https://doi.org/10.1016/j.cherd.2018.05.001.

[47]   A.P. Karttunen, H. Wikström, P. Tajarobi, M. Fransson, A. Sparén, M. Marucci, J. Ketolainen, S. Folestad, O. Korhonen, S. Abrahmsén-Alami, Comparison between integrated continuous direct compression line and batch processing – The effect of raw material properties, Eur. J. Pharm. Sci. 133 (2019) 40–53. https://doi.org/10.1016/j.ejps.2019.03.001.

[48]   Z. Mirza, J. Liu, Y. Glocheux, A.B. Albadarin, G.M. Walker, C. Mangwandi, Effect of impeller design on homogeneity, size and strength of pharmaceutical granules produced by high-shear wet granulation, Particuology. 23 (2015) 31–39. https://doi.org/10.1016/j.partic.2014.12.009.

[49]   J. Drelich, J.D. Miller, R.J. Good, The Effect of Drop Size on Advancing and Receding Contact Angles for Heterogeneous and Rough Solid Surface as Observed with Sessile Drop and Captive Bubble Technique, J. Colloid Interface Sci. 179 (1996) 37–50. https://ac.els-cdn.com/S0021979796901861/1-s2.0-S0021979796901861-main.pdf?_tid=37ccd566-b364-11e7-8c09-00000aacb360&acdnat=1508263047_5a188bc0aacd8c131d7bde94de35a89c (accessed October 17, 2017).

[50]   T.H. Muster, C.A. Prestidge, Application of time-dependent sessile drop contact angles on compacts to characterise the surface energetics of sulfathiazole crystals, Int. J. Pharm. 234 (2002) 43–54. https://doi.org/10.1016/S0378-5173(01)00949-8.

[51]   T.T. Chau, A review of techniques for measurement of contact angles and their applicability on mineral surfaces, Miner. Eng. 22 (2009) 213–219. https://doi.org/10.1016/j.mineng.2008.07.009.

[52]   E. Nowak, G. Combes, E.H. Stitt, A.W. Pacek, A comparison of contact angle measurement techniques applied to highly porous catalyst supports, Powder Technol. 233 (2013) 52–64. https://doi.org/10.1016/j.powtec.2012.08.032.

[53]   M. Thakker, V. Karde, D.O. Shah, P. Shukla, C. Ghoroi, Wettability measurement

apparatus for porous material using the modified Washburn method, Meas. Sci. Technol. 24 (2013) 125902. https://doi.org/10.1088/0957-0233/24/12/125902.

[54] J.B. Rosenholm, Liquid spreading on solid surfaces and penetration into porous matrices: Coated and uncoated papers, Adv. Colloid Interface Sci. 220 (2015) 8–53. https://doi.org/10.1016/j.cis.2015.01.009.

[55] A. Bahrami, M.I. Pech-Canul, C.A. Gutiérrez, N. Soltani, Wetting and reaction characteristics of crystalline and amorphous SiO2derived rice-husk ash and SiO2/SiC substrates with Al-Si-Mg alloys, Appl. Surf. Sci. 357 (2015) 1104–1113. https://doi.org/10.1016/j.apsusc.2015.09.137.

[56] C. Wang, M. Geramian, Q. Liu, D.G. Ivey, T.H. Etsell, Comparison of different methods to determine the surface wettability of fine solids isolated from Alberta oil sands, Energy and Fuels. 29 (2015) 3556–3565. https://doi.org/10.1021/ef502709r.

[57] R. Holm, S. Borkenfelt, M. Allesø, J.E.T. andersen, S. Beato, P. Holm, Investigation of surface porosity measurements and compaction pressure as means to ensure consistent contact angle determinations, Int. J. Pharm. 498 (2016) 355–361. https://doi.org/10.1016/j.ijpharm.2015.12.022.

[58] M.V. Hammes, A.H. Englert, C.P.Z. Noreña, N.S.M. Cardozo, Effect of water activity and gaseous phase relative humidity on microcrystalline cellulose water contact angle measured by the Washburn technique, Colloids Surfaces A Physicochem. Eng. Asp. 500 (2016) 118–126. https://doi.org/10.1016/j.colsurfa.2016.04.018.

[59] A. Alghunaim, B.M. Zhang Newby, Influence of tube wettability on water contact angle of powders determined by capillary rise, Colloids Surfaces A Physicochem. Eng. Asp. 492 (2016) 79–87. https://doi.org/10.1016/j.colsurfa.2015.12.010.

[60] A. Alghunaim, S. Kirdponpattara, B.M.Z. Newby, Techniques for determining contact angle and wettability of powders, Powder Technol. 287 (2016) 201–215. https://doi.org/10.1016/j.powtec.2015.10.002.

[61] A.L. Mundozah, J.J. Cartwright, C.C. Tridon, A.D. Salman, M.J. Hounslow, Wetting of binary powder mixtures, Int. J. Pharm. (2019) 118770. https://doi.org/10.1016/j.ijpharm.2019.118770.

[62] A.B.D. Cassie, Contact angles, Discuss. Faraday Soc. 3 (1948) 11. https://doi.org/10.1039/df9480300011.

[63] T. Gao, A.S.S. Singaravelu, S. Oka, R. Ramachandran, F. Štepánek, N. Chawla, H.N. Emady, Granule formation and structure from single drop impact on heterogeneous powder beds, Int. J. Pharm. 552 (2018) 56–66.

https://doi.org/10.1016/j.ijpharm.2018.09.036.

[64] S.T. Nase, W.L. Vargas, A.A. Abatan, J.J. McCarthy, Discrete characterization tools for cohesive granular material, Powder Technol. 116 (2001) 214–223. https://doi.org/10.1016/S0032-5910(00)00398-3.